Exogenic forcing and autogenic processes on continental divide location and mobility

Moodie, Andrew J.[1], Pazzaglia, Frank J.[2], and Berti, Claudio[2]

[1] *Department of Earth Science, Rice University, Houston, TX 77005*

[2] *Department of Earth and Environmental Sciences, Lehigh University, Bethlehem, PA 18015*

1.0 Abstract

The position and mobility of drainage divides is an expression of exogenic landscape forcing and autogenic channel network processes integrated across a range of scales. At the large scale, represented by major rivers and continental drainage divides, the organization of drainage patterns and divide migration reflects the long-wavelength gradients of the topography, which are exogenically influenced by tectonics, isostasy, and/or dynamic topography. This analysis utilizes long-wavelength topography synthesized by a low-pass filter, which provides a novel framework for predicting the direction of divide movement as well as an estimate of the ultimate divide location, that is complementary to recent studies that have focused on the χ channel metric. The Gibraltar Arc active plate boundary and Appalachian stable plate interior, two tectonically diverse settings with ongoing drainage system reorganization, are chosen to explore the length scales of exogenic forcings that influence continental drainage divide location and migration. The major watersheds draining both the active and decay-phase orogens studied here are organized by topographic gradients that are expressed in long-wavelength low-pass filtered topography ($\lambda \geq 100$ km). In contrast, the river network and divide location is insensitive to topographic gradients measured over filtered wavelengths < 100 km that are set by local crustal structures and rock type. The lag time between exogenic forcing and geomorphic response and feedbacks cause divide migration to be unsteady, and occur through pulses of drainage capture and drainage network reorganization that are recorded in sedimentological, geomorphic, or denudation data.

2.0 Introduction

Exogenic forcings such as climate, tectonics, eustasy and dynamic topography define the boundary conditions for a drainage network, and collectively determine the topographic gradients, drainage area, and hydrology of the system. Both in response to and independent of exogenic forcing, the internal autogenic processes of the linked hillslope-channel network, such as landslides, sapping, and avulsions drive system dynamism which further modifies the channel network configuration and evolution (Hajek & Straub, 2017). Continental divides, and their mobility, are an integrated expression of those responses and feedbacks between exogenic forcing and autogenic processes at a large scale. Exogenic drivers are most apparent in the active tectonic setting, where traditional views hold that the drainage divide develops along the spine of highest topography because of the strong coupling between surficial and tectonic processes (Beaumont *et al.*, 1992; Zeitler *et al.*, 2001a,b). In the absence of tectonic forcing, divide location and migration (Gilbert, 1877) becomes increasingly dependent on rock-type (Hack, 1982; Prince *et al.*, 2010, 2011), the thermo-chemical evolution of isostatically compensated topography (Fischer, 2002), and dynamic forces in post-orogenic landscapes (Mitrovica *et al.*, 1989; Young, 1989; Forte *et al.*, 1993; Gurnis *et al.*, 2000; Wegmann *et al.*, 2007; Moucha *et al.*, 2008; Flament *et al.*, 2013), all of which act to locally and regionally change topography and topographic gradients. More recently and in contrast, there has been an emerging focus on autogenic processes and feedbacks in headwater streams that may play a previously under-appreciated role in divide location and migration, even in post-orogenic landscapes (Perron et al., 2008; 2009; Willett et al., 2014; Hajek & Straub, 2017; Whipple et al., 2017a,b). In either case, having a conceptual model for how drainage divides are organized and migrate at the continental scale has profound implications for interpretations of delivery of sediment to the world's oceans and the construction of stratigraphic packages on both active and passive margins.

In both tectonically active and decaying orogens, there are curious examples of where the continental divide is not co-located with the highest mountain peaks (Hack, 1979; 1982; D'Agostino *et al.*, 2001) but rather follows the regionally highest-standing topography, defined by a topographic sub-envelope map (Hack, 1982), which a recent study coins as "drainage conformity to topography" (Black *et al.*, 2017). An excellent example of this drainage conformity to topography at the continental scale is illustrated by the drainage of the Rocky Mountains in the American west superimposed on a low-pass filtered rendering of the topography (Fig. 1), which isolates the long-wavelength components of the landscape (Wegmann *et al.*, 2007). The landscape shows a bi-radial drainage pattern away from two regionally-high foci defined by Yellowstone and Central Colorado (Fig. 1), regions where the landscape is know to be dynamically supported (Pierce & Morgan, 1992; Karlstrom *et al.*, 2012). The actual continental divide (black line in Fig. 1) snakes from north to south through this landscape, bisecting the high foci and locally traversing high-standing, but low-relief basins such as the Great Divide Basin (GDB, Fig. 1), far from the highest peaks or the most rugged topography. The actual divide is largely coincident with a "synthetic divide" that is drawn along the crest of the low-pass filtered long-wavelength topography (dashed blue line in Fig. 1; Wegmann *et al.*, 2007); the synthetic divide thus delineates the hypothetical drainage divide of the long-wavelength landscape There are places where the actual and synthetic divide separate, but it is not clear how to interpret the separation in terms of the exogenic forcings and autogenic processes that move divides.

These observations in the North American interior and elsewhere lead us to the central idea that we wish to explore in this paper: that the main check on continental divide location and divide migration is the gradient of the regional topography, as influenced by exogenic tectonic, isostatic, or dynamic topography drivers. We recognize that at the channel scale, the continental divide is defined by opposing channel heads influenced by autogenic fluvial, debris flow, sapping, and hillslope processes, but argue that these processes are not completely independent from the regional-scale exogenic drivers. To make our point that divide location and migration are primarily influenced by exogenic drivers, we explore the length scales characteristic of exogenic forcings and autogenic processes. We define what we mean by regional topography and gradients, and compare coordination between regional-scale observations and the location and migration of continental divides in the active Gibraltar Arc plate boundary and Appalachian Mountains stable plate interior settings.

3

3.0 Drainage divides, synthetic divides, and exogenic drivers vs. autogenic processes causing divide migration

Opposing topographic gradients in the hillslope and channel systems separated across a divide are widely recognized as the key determinant in divide stability or migration (Gilbert, 1877). Those gradients are changed by exogenic and autogenic forcings, but the subsequent channel network response is a complex problem and a topic of spirited current debate in the literature (Willett *et al.,* 2014; Yang *et al.,* 2015; Ruetenik *et al.,* 2016; Whipple *et al.,* 2017a,b). Channel network responses integrate along the entire channel length, through variable climatic and lithological factors including rock uplift and erosion rates, and thus dictate the channel elevation rise from a common base-level to the channel heads (Howard & Kerby, 1983; Howard, 1994; Whipple & Tucker, 1999; Snyder *et al.,* 2000; Crosby & Whipple, 2006; Supplementary Material).

If opposing channel-heads lie on a divide that is topographically symmetric at the scale of the entire drainage network including where it reaches a common base level, the divide location will be stable (Gilbert, 1877), even if reach-length channel gradients are not equal. In this case, the crest of low-pass filtered topography (e.g., Fig. 1) mirrors actual topography at all wavelengths. In contrast, when opposing channel heads lie astride a divide that is topographically asymmetric with respect to the scale of the entire drainage network including where it reaches a common base level, the asymmetry defines a gradient imbalance in favor of the shorter path to base level (Gilbert, 1877), even for the case where the opposing hillslopes along the crest of the divide may have equal gradients (Roering *et al.,* 1999). Low-pass filtered topography sees the topographic asymmetry at the scale of the entire drainage network graded to a common base level. Accordingly, continental divides migrate away from their shorter paths to base level and in the process remove the long-wavelength topographic asymmetry.

The steady-state long profiles of rivers flowing to the same base level on opposing sides of a drainage divide, which reflect the balance of erosional response to non-uniform uplift and rock-type (Willett *et al.,* 2014), provides a corollary measure of continental divide stability that can also be compared to low-pass filtered topography. The distance-elevation relationship of channels flowing to a common base level is best visualized using the χ (chi) linear

4

transformation of stream long profiles (Harkins *et al.*, 2007; Perron & Royden, 2013),

$$\chi = \int_{x_b}^{x} \left(\frac{A_0}{A(x)}\right)^{\theta} dx \qquad (1),$$

where x_b is the starting point on the long profile (base-level), x is upstream distance along the long profile, θ is the profile concavity, A_0 is a reference area (typically unity), and $A(x)$ is contributing drainage area upstream of any point x on the profile. This linear transformation of a stream long profile identifies where, along a divide, opposing streams are at disparate elevations and thus poised to capture or to be captured through divide migration (Willett *et al.*, 2014).

Opposing channel-head elevation differences can arise from exogenically-driven non-uniform uplift, essentially tilting or doming. In this case, contrasting χ values arise from the fact that the actual drainage divide is offset from the highest standing long-wavelength topography. An excellent example of this condition is illustrated by the drainage network of the greater Yellowstone region (Fig. 2; Wegmann *et al.*, 2007) that reflects a landscape shaped by active tectonics, glaciation, and differential erosion to rocks of variable hardness. The greater Yellowstone topography is dynamically supported by ascending warm mantle of the Yellowstone hotspot, forming a broad topographic bulge northeast of Yellowstone National Park, that sweeps westward like a wake defining the flanks of the Snake River Plain (Pierce & Morgan, 1992; Fig. 2A).

Following the method of Wegmann *et al.* (2007), the long-wavelength topography of the region is disconnected from short-wavelength relief, and a synthetic drainage divide that reflects a hypothetical drainage of this filtered landscape is defined along the crest of the long-wavelength topography (Fig. 2B). The actual divide aligns well with regional topography (i.e., the synthetic divide) in the west of the greater Yellowstone region. Toward the east, moving up the Snake River Plain and the regional elevation gradient produced by the Yellowstone hotspot, the actual drainage divide becomes offset from the highest standing topography. This offset progressively increases to the area of Yellowstone National Park, where the actual divide is significantly offset to the west of the crest of the long-wavelength topography (Fig. 2B). East-

 5

flowing Missouri headwater channels are uplifted by the regional dynamic support and find themselves at a higher elevation and having greater χ values than west flowing Snake River headwater channels which have comparatively lower χ values (Fig. 2C). In this case, both the unequal χ values and the separation of the actual and synthetic divides predict that the Snake River drainage is growing at the expense of the Missouri River drainage. There are numerous examples of divide mobility in this landscape, such as drainage captures and windgaps, that are the result of the stream network dynamically adjusting to exogenic land-surface deformation and climate change applied at several spatial and temporal scales (Anderson, 1947; Sears, 2009; Link & Hodges, 2011). Nonetheless, a clear pattern of separation of the actual and synthetic divides emerges from the analysis. As the dynamic support wanes westward at a given location from the passage of the Yellowstone hotspot, geomorphic processes drive the actual divide to migrate to the position predicted by the synthetic divide, and the two eventually coincide. Where dynamic support is recent and ongoing, there is offset of the long-wavelength topography from the actual divide, as geomorphic process lag in adjusting the landscape to reflect the position of the synthetic divide (Wegmann *et al.*, 2007).

In contrast to this case of exogenic landscape deformation, it is also possible that the equilibrium channel-head elevation and χ of opposing rivers could differ strictly because of autogenic river network geometry, topology, and channel substrate factors (Willett *et al.*, 2014). If this was the case for Yellowstone, low-pass filtering of the topography would not reveal a synthetic divide systematically offset from the actual divide, and contrasting χ values would be found across divides that align with the regional reconstruction of long-wavelength topography. The northwest side of the mapped Snake River Plain (Fig. 2) illustrates where autogenic factors might lead to unequal χ values in the opposing headwater streams.

Actual drainage divide stability or migration, in the context of k_s, χ, and synthetic divides, is demonstrated by numerical landscape evolution models predicated on the stream power equation that show how opposing channel-head elevations across a divide tend to quickly stabilize through both positive and negative autogenic feedbacks unless exogenically perturbed (Tucker & Hancock, 2010; Ruetenik *et al.*, 2016; Whipple *et al.*, 2017b). For example, when the drainage area of one basin grows through the process of stream capture, channel incision and

6

hillslope erosion increase in the growing basin, and decrease correspondingly in the pirated basin that has lost drainage area. This adjustment is a positive feedback that accelerates divide migration and expansion of the growing basin (Yang *et al.*, 2015). In contrast, decreased erosion rates in the pirated basin change the balance of rock uplift and erosion, causing the basin with drainage loss to experience surface uplift and steepening, thereby increasing erosion and decelerating divide migration.

The competition between the positive and negative autogenic feedback mechanisms, and thus distribution of χ along a continental divide, ultimately depends on the channel response time (Whipple *et al.*, 2017b), something that we do not explicitly explore in this paper. Rather we assert, following from work in diverse active tectonic (D'Agostino *et al.*, 2001), intracontinental passive margin (Hack, 1979; 1982; Judson, 1975; Young, 1989), and dynamic topographic (Wegmann *et al.*, 2007) settings, that autogeneic mechanisms are playing out on all divides within a watershed but at the largest scale, that of the continental divides, it is the exogenic processes alone that are able to drive persistent divide migration that is independent of local topographic roughness and local gradients. Our study areas allow us to explore the threshold length scale where exogenic processes emerge as in important signal above the autogenic noise, and speculate on what lithospheric-scale processes may be driving that forcing.

Ultimately, the landscape observable we exploit to suggest whether a divide is migrating or poised to migrate in response to a lithospheric-scale tectonic forcing is the deviation (separation) between the actual divide and the predicted stable divide location determined by the synthetic divide and long-wavelength topography. Numerical modeling suggests that this separation is transient (Ruetenik *et al.*, 2016), but it provides a starting point for quantifying the degree of drainage basin disequilibrium in an orogen-scale landscape.

4.0 Study areas

We chose two diverse settings with ongoing drainage system reorganization (see references below) to explore the dependence of drainage divide migration on exogenic lithospheric-scale tectonic, isostatic, and dynamic topography forcing (Fig. 3). Both study areas offer insights into the lag time between exogenic forcing and geomorphic system response, represented by recent shifts in their respective continental divides.

The Gibraltar Arc of southern Spain and northern Morocco (Fig. 3A), offers an active tectonic setting where slab rollback and lithospheric delamination in a west-migrating subduction zone (Lonergan, 1993; Lonergan & White, 1997; Garcia-Castellanos & Villaseñor, 2011; Platt *et al.*, 2013; Bezada *et al.*, 2013; 2014) produces an east-west temporal gradient in topographic adjustment to dynamic support of the lithosphere (Garcia-Castellanos & Villaseñor, 2011; Palomeras *et al.*, 2014). Drainage reorganization in the Gibraltar Arc is asymmetric across the northern and southern sections of the Arc, and leaves behind a record of drainage capture and integration in the landscape morphology (Harvey & Wells, 1987; García *et al.*, 2004; Reinhardt *et al.*, 2007; Maher & Harvey, 2008; Schulte *et al.*, 2008; Pérez-Peña *et al.*, 2009).

In contrast, the Appalachian Mountains and foreland, embedded in the passive margin of eastern North America (Fig. 3B), offers a post-orogenic, intraplate setting (Hack, 1979; 1982) with a well-studied post-rift geodynamic evolution (Wilson, 1966; Oliver *et al.*, 1983; Sheridan & Grow, 1988; Faill, 1997a,b) where the long-term decay of the topography is documented in diverse datasets (Pazzaglia & Brandon, 1996; Matmon *et al.*, 2003; McKeon *et al.*, 2013; Portenga *et al.*, 2013) and where the landscape is currently being uplifted by a dynamic topography response to the foundering of the Farallon slab (Moucha *et al.*, 2008; Rowley *et al.*, 2013; Moucha & Reutenik, 2017).

Rock-types are diverse in both settings, ranging from hard crystalline rocks to poorly consolidated sediments, but it is the overall climatic differences and duration of weathering based on relative age of the Gibraltar Arc and Appalachian landscapes that introduces notable variation in the dominant erosion processes. The relatively drier Mediterranean climate and active orogenic setting of the Gibraltar Arc results in more exposed bedrock, particularly for carbonates and crystalline rocks, and thin colluvial mantles in comparison to the Appalachians. Less competent units are prone to mass movement in the relatively steeper Gibraltar Arc landscape (Sanz de Galdeano & Lopez-Garrido, 1999; Reinhardt *et al.*, 2007). In contrast, the humid-temperate climate and post-orogenic setting of the Appalachian landscape favors a soil-mantled, creep-dominated landscape with comparatively fewer landslides and bedrock that has been locally deeply weathered into saprolite (Pavich, 1989; Ciolkosz *et al.*, 1990).

8

5.0 Methods and data sources

We apply a general methodology, following from Wegmann *et al.* (2007), to the contrasting tectonically active and stable settings of the Gibraltar Arc and the Appalachians, respectively. We start with a continuous topographic and bathymetric digital elevation model, that is subjected to filtering to isolate regional from local elevation gradients. We use the 30 arc-second General Bathymetry Chart of the Oceans (GEBCO 2008; http://www.gebco.net/data_and_products/gebco_digital_atlas/) that contains a seamless transition from bathymetry to similar-resolution topography derived from one-kilometer averages of the US Geological Survey SRTM30 dataset (http://www.gebco.net/; http://www2.jpl.nasa.gov/srtm/). The digital data are assembled in ESRI ArcGIS 10.x and manipulated in ArcGIS as well as in the Generic Mapping Tools (GMT; Wessel & Smith, 1991) 5.x. Example GMT bash scripts used in the analysis are provided in the supplementary material.

Determining the location of the drainage divides (both actual and synthetic) uses common and well accepted work-flows in the ArcGIS Spatial Analyst Toolbox. Digital elevation models (DEMs) are processed to find flow directions and accumulations, defining the stream network and drainage basins. The drainage divides are identified as lines of contact between opposing drainage basins, in essence the line tangent to the basins where flow accumulation is zero. The actual drainage divides are derived from the GEBCO 2008 DEM. This work-flow remains the same for the development of the synthetic divide from a filtered DEM. Therefore, the synthetic divide (Figs. 1 and 2) represents the objectively located axis of highest standing topography of an input DEM. Uncertainty in the position of the derived drainage divides is a function of the grid spacing in the underlying DEM; where the ~1 km grid spacing of the GEBCO 2008 DEM sets the maximum uncertainty as the distance between diagonally adjacent grid cells (1.41 km). For this study, this uncertainty is assumed to be the same for both the actual and synthetic divides.

The structure and scale of deep Earth features and exogenic processes that drive surface uplift dynamism in the Gibraltar Arc and Appalachian Mountain settings are constrained by several geophysical datasets. These include the Earth Gravitation Model 2008 (EGM2008 or EGM), the isostatic (Simpson *et al.,* 1986) and Bouguer (Simpson *et al.,* 1987; Kucks, 1999)

9

gravity maps of the conterminous United States, CRUST 1.0 (http://igppweb.ucsd.edu/~gabi/rem.html; Laske, *et al.*, 2013), and site-specific estimates of crustal and lithospheric thickness (Fullea *et al.*, 2010; Hawman *et al.*, 2012; Wagner *et al.*, 2012). We extract cross sections through the crustal and lithospheric models of the Gibraltar Arc (Fig. 4) and the gravity data of the Appalachians (Fig. 3B) to determine the wavelength of thickness variations of the crust and lithosphere to inform our topographic filtering criteria. The half wavelength of variations in the geophysical datasets is selected as a maximum filtering wavelength, so as to always retain the first-order of scales of variation (i.e., the full wavelength) in the filtered topography. We find that in the Gibraltar Arc, the half wavelength of the crustal and lithospheric thickness is ~150 km, whereas the corresponding geoid variations have a half wavelength of ~100 km. In the Appalachians, the half-wavelength of crustal thickness is ~100 km. Two filter thresholds are thus selected as 150 and 100 km. We complement these two long-wavelength filtering windows with a shorter, 50 km filter window that is able to capture potentially uncompensated crustal-scale features, such as ranges and valleys controlled by rock type or local structural deformation.

5.1 Filtering of digital data

We low-pass filter a DEM at various wavelengths to obtain a surface that crudely matches the wavelengths represented by crustal and lithospheric thickness and structure. We adopt a methodology described in Wegmann *et al.* (2007) using a Fast Fourier Transform (FFT) function in GMT. For this analysis, topography is converted from the spatial domain to the frequency domain where we are able to pass low frequencies (long wavelengths) and eliminate high frequencies (short wavelengths), followed by conversion back to the spatial domain. We smoothly taper the transition between the frequencies that are retained and those that are cut with a cosine function. A typical cosine taper corresponds to a smooth transition of 10 km between the wavelengths that are cut and those that are retained. The input DEM area extends beyond the study regions, such that edge effects produced during the filtering are minimized.

The output from this process is a new, smooth rendering of the topography that we use to define the synthetic divide, employing the routine described above. The location of the synthetic divide can be visually and quantitatively compared to the actual divide defined by the short-

10

wavelength topography presented in the unfiltered DEM (i.e., the actual topography) to produce a measure of divide separation.

5.2 Quantifying actual and synthetic divide separation

In order to quantitatively assess the respective locations of the actual and synthetic divides we calculate the deviation (km), and the root-mean-square deviation (RMSD) (km) for each filtered wavelength. A Matlab script (included in supplementary information) is used to determine the minimum separation between the synthetic and actual divide for each point along the actual divide. Said another way, the deviation distance is a quantification of how far away the synthetic divide is from the actual divide, at any point along the length of the actual divide. A calculated deviation of zero, therefore, represents no separation, or a spatial overlap between the actual and synthetic divides. The along-divide reference frame generated by this method is helpful for assessing divide deviation at the regional scale, but local sinuosity of the actual drainage divide precludes a meaningful interpretation of local fluctuations in the deviations of the divides.

Deviation distance is calculated as geodesic distance along a great-circle between two points by use of the haversine formula for a sphere with an average radius of the Earth (6371 km). Before calculation, all divides are resampled following a bisection routine to create point spacing of approximately 500 m, however, the calculation is relatively insensitive to reductions in point spacing beyond ~2 km. Minimum deviation between actual and synthetic divides is only calculated over the range of latitudes or longitudes for which the synthetic divide is mapped in each study setting, for north-south trending divide and east-west trending divides, respectively. The root-mean-square deviation (RMSD) is then calculated for each of the synthetic divides by

$$\mathrm{RMSD} = \sqrt{\frac{\sum_{i=1}^{n} D_i^2}{n}} \qquad (2),$$

where n is the number of calculation points along the length of the actual divide, and D_i is the devation calculated for the i^{th} point along the actual divide.

The RMSD (retaining the units of length) therefore represents a normalized aggregate of all the deviation measurements over the length of the divide. Where the synthetic divide locally deviates from the actual divide by less than the RMSD calculated for that synthetic divide, the divides are statistically overlapping and the opposite case, where the local deviation is above the RMSD, the divides are statistically different with the magnitude of the difference crudely scaling linearly with deviation. Among the 50- 100- and 150-km wavelength synthetic divides, the smallest RMSD value can then be interpreted as the best overall fit to the actual divide, and the largest RMSD can be interpreted as the worst overall fit to the actual divide.

Surface denudation data from each study area were projected onto the actual divide for comparison with divide deviation in the along-divide reference frame. This projection is simply made along a line of latitude or longitude, for north-south trending or east-west trending divides respectively. Where the divide crosses the same latitude or longitude two or more times, the first intersection of a latitude or longitude line and the actual divide, in the along-divide reference frame, is the selected projection point for erosion data existing at that line of latitude or longitude. Projecting the data in this manner is an objective method to crudely compare the scaling between erosion rates and the divide deviation.

5.3 Simulated topography example

We present here a simulated landscape (Fig. 5) to apply our methods to in order to demonstrate the application and utility of our approach in evaluating divide migration potential. We start with a broad, shallowly-sloping 2000 km x 2000 km landscape with two prominent parallel ridges and variable-sized randomly-generated topography and roughness elements (i.e., hills) generated with a Matlab script (included in supplementary material). The analysis shows only the centered 1000 x 1000 km square-shaped region, to reduce edge effects of the filtering method in the interpretation of the results (Fig. 5A). The landscape tilt is toward a shoreline (i.e., the theoretical base-level, where elevation = 0) positioned on the western edge of the simulated topography, and so the actual continental drainage divide is situated on the western-most of the two parallel ridges, following the ridge-axis, directly from north to south (thick black line, Fig.

12

5A). A hypothetical drainage channel network is hand-drawn to the topography of the simulated landscape. The initial topography used in this simulated topography example is one specific landscape configuration, and so the exact results are expected to change given different topography. However, this simulated topography example is useful for demonstrating the method applied to a common landscape configuration: ridges trending sub-parallel to a shoreline that sets the base-level for a drainage network actively dissecting the high-standing topography. For example, the topography in the Gibraltar Arc and Appalachian study settings crudely exhibit this landscape configuration (Fig. 3).

West of the continental drainage divide, dendritic drainage networks head in the westernmost ridge and flow west to base-level at the shoreline (e.g., channels 1 and 2, Fig. 5A). In contrast, the southward-directed plunge of the eastern ridge creates a narrow, north-south valley and a more trellis or rectilinear drainage pattern that drains off to the east (channels 3 and 4, Fig. 5A). A dotted line shows a local drainage divide between channel networks 3 and 4. Assuming uniform rock-type which is not realistic for a landscape with these embedded ridges, but a useful thought experiment nonetheless, a calculation of the χ values along the channel networks would reveal relatively high values in the headwaters of channel 3, compared to channels 1, 2, and 4; the stream segments in Fig. 5A are colored according to expected (but not computed) χ values. The χ metric alone would suggest migration of the drainage divides (e.g., Willett *et al.*, 2014), with channel networks 1, 2, and 4 all poised to capture the drainage of channel 3.

The simulated landscape is filtered at 150 km to eliminate the relatively small-scale roughness from the landscape and isolate the long-wavelength components of the topography (Fig. 5B). The filtered topography retains the regional east-west gradient in the landscape, but the two parallel ridges are reduced to one broad ridge following roughly the same axis. The synthetic divide, following the central axis of this filter-produced ridge (dashed blue line in Fig. 5B), however, lies to the east of the actual continental drainage divide (solid black line in Fig. 5). The long north-south drainage (channel 3 in Fig. 5B) is now mostly west of the synthetic divide. This observation suggests that channels 1 or 2 have a competitive advantage, with respect to channel 4, in capturing the headwaters of channel 3, and thus redirecting its flow to the west.

This experiment illustrates two important points. First, is the effective segregation of

13

long-wavelength topography from smaller-scale, short-wavelength topographic features. Landscape features smaller than the low-pass filter wavelength, e.g., the minor variable-sized randomly-generated roughness, are removed from the landscape and have no role in determining the location of the synthetic divide. The filtered topography is dominated by the regional east-west landscape gradient, the location of the now-merged parallel ridges, and some local influence from larger hills.

Second, is the ability to recognize regional scale patterns in topography through the noise of shorter-wavelength features. Imagine that the valley between the two parallel ridges in the simulated topography represents a fault-bounded graben or strike valley underlain by soft rocks. Lower-order channels will respect the local topographic gradients imposed by this short-wavelength, structurally or rock-type controlled ridge and valley topography (channel 3), but the higher-order trunk streams must respect the regional topographic gradient and flow off to the east or the west. The synthetic divide produced by our methodology identifies the long-wavelength regional topographic gradients, so, despite being in a valley, the headwaters of channel 3 ends up being the most stable location of the continental-scale drainage divide. We assert that in this case, it is the topological peculiarities of the drainage network, responding to local topography, that have lead to the separation of the actual and synthetic divides. Alternatively, if the ridges in Fig. 5 were being actively built by some geologic process, such as faults, then the separation of the actual and synthetic divides and the drainage network itself is an exogenically-driven reality. In both cases, over time, the continental divide would eventually migrate eastward to the location of the synthetic divide, driven by autogenic and stochastic geomorphic processes playing out in the headwaters of the drainages.

5.4 χ transformation stream power mapping

The χ transformation of stream long profiles is useful for the visualization of disequilibrium in channel-head elevation and stream power across a drainage divide (Harkins *et al.*, 2007; Perron and Royden, 2013). The calculation of the χ values follows the integral approach of Perron and Royden, 2013, as implemented by the TopoToolbox 2 topographic analysis tools for Matlab (Schwanghart and Scherler, 2014).

 14

The stream network used in the χ calculation is derived from the same ~1 km grid-spacing GEBCO 2008 DEM used elsewhere for topographic elevation data in this analysis. All stream networks derived, analyzed, and plotted within the analysis have their base-level (x_b in Equation 1) as modern sea-level. Thresholding of the stream network at the headwaters of streams was limited to a minimum contributing area of 20, 200, and 100 km^2 for the Gibraltar Arc, Appalachians, and Yellowstone study areas, respectively. A constant profile concavity index $\theta = 0.45$ and reference area $A_0 = 1 \times 10^6$ m^2 (1 km^2) are used in the evaluation of Equation ~~7~~1 for each stream network identified within the study area. The χ value is calculated along the channel network at every DEM cell node (every 1–1.4 km stream-wise) and data are then aggregated into approximately 20 km stream segments by averaging, in order to aid in visual interpretation of the results.

The input DEMs are transformed into Universal Transverse Mercator projections centered on each study area (UTM zones 30, 17, and 12 for the Gibraltar Arc, Appalachians, and Yellowstone, respectively). This transformation to a projected coordinate system introduces an area distortion, especially on the fringes of the analysis. In the case of Yellowstone and the Appalachians, some streams of interest have headwaters at the continental drainage divide, yet a distal base-level at the outlet of the Mississippi River; this requires calculation of χ over a substantial channel length that samples contributing upstream areas along the channel that are subject to variable area distortions from the map projection. The area distortion on the fringes of the present analysis of the Yellowstone and Appalachian study areas is expected to be small, on the order of a few percent at most (discussed in detail in the supplementary material). The magnitude of differences in calculated χ values across divides that are used as a qualitative tool for identifying disequilibrium (e.g., Willett *et al.*, 2014), is large with respect to the uncertainty in the calculation and the area-distortion error, and therefore inconsequential to interpretations made from the χ maps. An additional error may be introduced by the vertical position error of the underlying DEM, however at the scale of continental drainage divides, these positional errors are also small and ignored.

6.0 Results

The positions of the synthetic divide and the actual divide (and with respect to one another) are qualitatively described in this section and quantified by the local deviation, RMSD calculations, and χ as described above. All RMSD calculation results are in presented in Table 1.

6.1 Gibraltar Arc continental divide

The Gibraltar Arc low-pass filtered results (Fig. 6A, B, and C) show a progressive deviation of the drainage divide from the synthetic divide with increasing filter wavelength, particularly in the southeast of Spain (Fig. 7A, B, Table 1). Tick marks on the drainage divides in Fig. 6 correspond to the cumulative along-divide distances that make the x-axis in Figs. 7 and 8, to spatially orient the reader across the figures. The synthetic divide derived from the 50 km filter aligns well with the actual divide in both the Spanish and Moroccan sections of the arc (Fig. 6A), mimicking the actual divide very well overall to the point that it follows the jagged north-south bends in the Betic Cordillera. This is further demonstrated by consistently small variations in the deviation calculations, and small RMSD values of 7.2 ± 0.6 and 6.9 ± 0.6 km for the Spain and Morocco sections, respectively (Fig. 7A, B).

When the 100 km low-pass filter is applied, the jagged north-south bends in the Betic Cordillera are reduced to two regional high-standing domes in the south-east of Spain (Fig. 6B). The synthetic divide generated from this filtered topography shows generally good alignment in the Moroccan section of the Gibraltar Arc, with just two sections of the synthetic divide (about 110 km total length) that are calculated to deviate with respect to the actual divide greater than the RMSD (10.7 ± 0.4 km) (Fig. 7B). In the Spanish section of the Gibraltar Arc, however, there is deviation of the synthetic divide from the actual drainage divide along most of its east-west extent from the Straits of Gibraltar through the Betic Cordillera (Fig. 7A), resulting in a RMSD of 17.1 ± 0.3 km, peaking at ~40 km of deviation as the synthetic divide moves into the high-standing valley of the Granada Basin. Near Sierra de los Filabres, the synthetic divide locally returns to the mapped actual divide but is shifted west into the high-standing valley of the Gaudix Basin, roughly where the actual divide turns north (Fig. 6B).

At the 150 km threshold filter (Fig. 6C), a good general alignment persists for the divides

16

in the Moroccan section of the Gibraltar Arc with small calculated deviation distances (Fig. 7B). However, the topographic expression of the Rif Range in Morocco dissolves into the Atlas Mountains at this filtered wavelength and the synthetic divide would bend south and east away from the Alboran Sea. The mapped synthetic divide (Fig. 6C) is therefore limited in eastern extent. The synthetic and actual divides align well for this length of mapped divide, which results in a small RMSD of 8.0 ± 0.5 km. Similarly for the Spanish section of the Gibraltar Arc, the Betic Cordillera has been reduced to one regional oblong dome of high-standing topography where alignment of the divides is good in the west but poorer in the east where deviation in the synthetic and actual divides grows considerably through the core of the Betic Cordillera (Fig. 7A) (RMSD = 16.3 ± 0.4 km). Despite this deviation, the RMSD of the 100 km filter, rather than the 150 km filter, remains the largest for the Gibraltar Arc study setting.

River terraces, river incision, basin erosion (Fig. 8A), and χ (Fig. 9A) vary with the RMSD for the Spanish part of the Gibraltar Arc. The highest river incision rates and basin wide erosion rates calculated by a range of methods integrating across short (Stokes *et al.*, 2002; García *et al.*, 2003; Pérez-Peña *et al.*, 2009; Azañón *et al.*, 2006; Bellin *et al.*, 2014) and long time scales (Weijermars *et al.*, 1985; Zeck *et al.*, 1992; Lonergan & Mange-Rajetzy, 1994; Johnson, 1997; Reinhardt *et al.*, 2007; Clark & Dempster, 2009; Vazquez *et al.*, 2011) are concentrated in the Sierra Nevada region where the RMSD is maximized (Fig 8A, Supplementary Table 1). Note that the data in Fig. 8A reflect only measurements that confidently record denudation due to geomorphic processes (in contrast to tectonic exhumation). Field observations in this region note a non-uniform distribution of river terraces in adjacent and opposing drainage basins moving along and across the divide, as well as wind gaps all consistent with active topologic changes in the drainage network (Calvache & Viseras, 1997; Mather, 2000; Stokes *et al.*, 2002; Stokes & Mather, 2003; Stokes, 2008; Berti *et al.*, 2014). Similarly χ values are consistently higher north of the divide, with the largest cross-divide differences lying along the ridge of Sierra Nevada (Fig. 9A) and continuing to the north and east. The χ value disparity across the ridge of Sierra Nevada is mimicked by hypsometric analysis of stream long profiles draining the range to the north versus those draining to the south (Azañón *et al.*, 2012; 2015).

17

6.2 Appalachian Mountains continental divide

Low-pass filtering of the Appalachian landscape (Figs. 6D, E, and F) shows deviation of the synthetic divide from the actual divide particularly at the 100 and 150 km wavelengths (Fig. 7C, Table 1). Again, the tick marks on the drainage divides in Fig. 6 correspond to the cumulative along-divide distance in Figs. 7 and 8. Major ridges, such as the Blue Ridge and those of the Ridge and Valley (Fig. 3B, inset) are preserved in the 50 km threshold filter (Fig. 6D) so here, the synthetic divide is aligned relatively well to the actual divide and the RMSD value is one third to half of that calculated for the longer wavelength filters (RMSD = 19.3 ± 0.4), and relatively small local deviation values (<30 km, Fig 7C). At the 100 km filter wavelength, individual ridges and valleys disappear and a spine of high topography that generally coincides with the southern Blue Ridge south of Virginia, and the center of the Appalachian foreland in and north of Virginia emerges (Fig. 6E). The synthetic divide follows this spine, and a dramatic deviation with the actual divide, herein called the James-Roanoke-New Rivers gap (JRN) is created. The JRN gap is represented in Fig. 7C by the region of high calculated deviation distances, roughly in the center portion of the divide, and is responsible for the overall high RMSD of 40.5 ± 0.2 km for this 100 km filter wavelength. Further south, the synthetic divide trends parallel to the southern Blue Ridge, and is consistently offset to the west of the actual divide. The JRN gap between the synthetic and actual divides in western Virginia persists in the 150 km filter (Fig. 6F); otherwise, the synthetic and actual divides show generally good agreement (Fig. 7C). The RMSD for the 150 km filter (29.2 ± 0.3 km) is less than that of the 100 km filter, but the patterns of offset between the synthetic and actual divide are similar. The high-standing long-wavelength Appalachian topography derived from the 150 km filter has steeper sloping flanks than the 100 km filter.

A large body of river incision and landscape erosion data assembled for the Appalachian Mountains over the past 25 years shows remarkable steadiness over different time scales, but local non-uniformity consistent with the Appalachian divide deviation and RMSD calculations (Pazzaglia *et al.,* 2015; Fig. 8B, Supplementary Table 2). Erosion rates derived from thermochronometry, terrestrial cosmogenic nuclide (TCN) alluvial and exposure ages, and suspended sediment concentrations consistently range from ~5 to 50 m/My (units are equivalent

18

to mm/kyr) with a mean of ~20 m/My (Reuter, 2005; Portenga *et al.*, 2013). Rates of river incision tend to be more variable than erosion and are locally more rapid in comparison to the erosion rates (Mills, 2000; Ward *et al.*, 2005). Locally, as at major knickzones like the Fall Zone, incision can be as rapid as 250 m/My, even into hard, crystalline rocks (Reusser *et al.*, 2004; 2006). Some of the lowest measured rates of erosion, based on bedrock terrestrial cosmogenic nuclides (TCN) exposure ages and drainage basin average alluvial TCN concentrations come from or near the JRN gap in the Blue Ridge and Appalachian Plateau provinces (Fig. 8B). The slow erosion rates contrast sharply with relatively rapid rates of river incision in the same region which tend to lie in the Blue Ridge and Ridge and Valley provinces of the JRN gap in the headwaters of the James River and its main tributaries that are currently incising into the sedimentary rocks of the Ridge and Valley between ~45 and ~160 m/My (Harbor *et al.*, 2005; Pazzaglia *et al.*, 2015).

In addition to patterns in erosion rates along the divide, the rates of erosion on opposite sides of the drainage divide may reflect a landscape poised for drainage capture. A spline surface is fit to all of the incision and erosion rate data compiled for the Appalachians, and subsequently sampled along three cross-divide transects that are strategically located near dense data clusters (Fig. 10A); additional detail on this method is included in the supplementary material. It is necessary to use measurements produced by a variety of methods in the spline surface fit (AHe, TCNa, TCNb), otherwise the surface is poorly constrained. While these data record geomorphological process that integrate across a range of time and space scales, the rates can be evaluated in aggregate to observe general trends in erosion rates along or across the divide. This approach reveals that there are generally lower erosion rates west of the actual divide, with local maximums near the divide for Transects 1 and 2 (Fig. 10B).

Appalachian divide χ values are consistently higher for the headwaters of west-flowing rivers with respect to their east-flowing Atlantic slope counterparts across the divide (Fig 9B). Specifically, in the JRN gap area, the New River has, at its headwaters, χ values approximately 2 times larger than the headwaters of the Roanoke and James Rivers across the divide. Pleistocene formation of the Ohio River and related base-level fall needs to be taken into consideration for the similarly high χ values in the headwaters of the Monongahela River north of the JRN gap,

19

where the deviation of the actual and synthetic divides is small.

7.0 Discussion

Our results indicate that the actual and synthetic continental divides are not uniformly co-located, and that the rates of erosion and river incision and χ values at the divides change in concert with the local deviations of the synthetic divide from the actual divide for both the Gibraltar Arc active plate boundary and Appalachian stable plate interior settings. In the context of the diverse rock types and structures that underlie these regions and the scale of the drainage networks and divides investigated, we interpret these results to mean that exogenic deformation of the land surface, driven by tectonic, isostatic, or dynamic topography processes is the primary reason for deviation of the synthetic and actual divides that establishes a long-wavelength topographic gradient across which the divides migrate. We explore these results of our study settings in detail, provide some insights on the gradients and length scales that influence drainage network topology, and compare our results to other regions that have also argued for exogenic controls on divide mobility.

7.1 The Gibraltar Arc

Evidence for river capture, drainage rearrangement, and basin integration has been documented for the Gibraltar Arc, particularly the Spanish section through the Betics and surrounding basins (Harvey & Wells, 1987; Mather, 2000; Stokes *et al.*, 2002; García *et al.*, 2004; Reinhardt *et al.*, 2007; Maher & Harvey, 2008; Schulte *et al.*, 2008; Pérez-Peña *et al.*, 2009). Erosion rates (Fig. 8A), river incision rates, and headwater χ values (Fig. 9A) offer some quantification for both recent movement of the divide as well as the potential for future migration. These data are no doubt influenced by the tectonic exhumation and local active faulting (Lonergan & Mange-Rajetzy, 1994; Johnson, 1997; Clark & Dempster, 2009; Vazquez *et al.*, 2011; Azañón, *et al.*, 2015) that determine the distribution of rock types of varying resistance exposed at the surface to erosion. Furthermore many of the compiled erosion data are focused in the regions of high relief. Nonetheless, the erosion, incision, and χ data scale roughly

20

with the divide deviation, showing high erosion rates and unequal χ values across the divide near Sierra Nevada, where divide deviation is largest. We interpret this to mean that in regions of lower erosion rates, the continental divide is more or less fixed in a stable position, driven back and forth by autogenic processes, but not moving in a particular direction. In contrast, exogenic tectonic or dynamic topography forcings drive divide migration in a particular direction, causing drainage captures, fluvial incision, and higher erosion in response to a changing base-level.

The active tectonic and dynamic topography processes documented for this region (Platt *et al.*, 2013) offer plausible mechanisms for driving continental divide migration. Recent studies on crustal thickness variations (Fullea *et al.*, 2010), subduction zone corner flow induced dynamic topography (Lonergan & White, 1997), and post-delamination isostatic rebound (Garcia-Castellanos & Villaseñor, 2011; Bezada *et al.*, 2013, 2014) provide the context for the long-wavelength topography development that ultimately generates the geomorphic potential responsible for driving drainage divide migration and drainage system reorganization. Maximum crustal thickness in the Spanish section of the Gibraltar Arc (Betic Cordillera) lies north of the actual drainage divide, about 20 km north of Sierra Nevada and coincident with the Granada Basin (Fig. 4B; Fullea *et al.*, 2010). In contrast, in the Moroccan section of the Gibraltar Arc (Rif range), the axis of maximum crustal thicknesses lies beneath the actual drainage divide for nearly the entire length of the section (Fig. 4B). The area of highest local deviation for the Spanish section of the divide is coincident with the location of the crustal root (Figs. 4B and 7A), which is thought to have developed during construction of the Betic Cordillera in the Tortonian. The correlation between crustal thickness and location of the long-wavelength topography suggests that isostatic processes related to the crustal root are an important control on divide location for the Gibraltar Arc.

Most geodynamic models of the Gibraltar Arc and Alboran Sea appeal to an east dipping subduction zone rolling back to the west through most of the Miocene (Lonergan & White, 1997; Rosenbaum *et al.*, 2002; Spakman & Wortel, 2004; Platt *et al.*, 2013; Bezada *et al.*, 2013). Subduction zone rollback here is postulated to generate a corner flow of warm and buoyant asthenosphere material that would produce dynamic support of the lithosphere and thus surface uplift. Because the rollback is time transgressive, the dynamic support and surface uplift would

21

have a surficial expression in a similarly west-migrating dynamic topography wave, analogous to what is documented for Yellowstone (Pierce & Morgan, 1992; Wegmann *et al.*, 2007). Following from the Yellowstone observations of divide separation and lag time of drainage system reorganization (Fig. 2), we would expect to find good agreement of the actual and synthetic divides in the eastern part of the Gibraltar Arc (i.e., small divide deviation values), with progressive offset toward the west, and overall north-south symmetry across the Alboran Sea. Instead, we found unpaired behavior of the Spanish and Moroccan segments of the divide, and a high calculated deviation distance for the eastern, rather than western part of the Betic Cordillera in Spain (Fig. 7A).

The patterns of divide deviation in the Gibraltar Arc are more consistent with a differential dynamic topography uplift imposed beneath the Betics more or less simultaneously, rather than as a migrating wave, forcing an earlier tectonically-inherited drainage pattern to rearrange and superimpose onto existing structures. We could interpret these results in the context of regional and nearly simultaneous lithospheric delamination (Seber *et al.*, 1996) with some component of convective removal of the lithosphere (Calvert *et al.*, 2000), rather than time-transgressive slab rollback. Details of one delamination model are provided by Seber et al. (1996), who propose that a tear in the subducting slab, decoupled from the base of the lithosphere, is sinking into the sub-lithospheric mantle. The sinking generates a warm asthenosphere return flow to buoyantly uplift the central and eastern section of the Betic Cordillera in the Spanish section of the Gibraltar Arc. Garcia-Castellanos & Villaseñor (2011) further this model, placing the tear point in the lithosphere about 50 km north-east of the Straits of Gibraltar and suggesting that the slab remains attached to the continental lithosphere below the Morocco section of the Gibraltar Arc, that the tear may have migrated from east to west following from Spakman & Wortel (2004), and that there is likely some component of ongoing isostatic adjustment where the slab is detatched. Similarly, Lis Mancilla *et al.* (2013) place the modern slab tear point a bit further east. Palomeras *et al.* (2014) alternatively propose a window in the sinking slab under the Betics, ending in the Málaga area. Independent of the details of any given geodynamic model, the results from our analysis are in better agreement with those that argue for delamination or a lithospheric window in the eastern and Spanish part of the Gibraltar Arc, rather than roll-back induced corner flow.

22

In summary, we could appeal to either variations in crustal thickness driven isostasy or slab-induced dynamic topography to explain the configuration of long-wavelength topography for the Gibraltar Arc. In both cases, the crest of the long-wavelength topography most notably deviates from the actual drainage divide in the eastern part of the Betics range in Spain. Accordingly, this is where there is ample geomorphic evidence for an actively migrating continental divide and changes in the drainage network topology.

7.2 The Appalachians

The continental divide in eastern North America is coincident with the Blue Ridge escarpment from South Carolina to southern Virginia, then steps westward from the Blue Ridge and Piedmont crystalline rocks into the sedimentary rocks of the Appalachian foreland north of the North Carolina (NC) – Virginia (VA) state line, and then west again into the relatively undeformed foreland sedimentary rocks of the Allegheny Plateau in Pennsylvania (PA) (Fig. 3B). Location and migration of this divide (Davis, 1903; Johnson, 1907, 1931; Meyerhoff & Olmsted, 1936; Thornbury, 1965; Meyerhoff, 1972; Hack, 1975; 1979; 1982; Pazzaglia & Brandon, 1996; Pazzaglia & Gardner, 1994; 2000; Spotila *et al.*, 2004; Harbor *et al.*, 2005; Gunnell & Harbor, 2010; Prince *et al.*, 2010, 2011; Bossu *et al.*, 2013, Gallen *et al.*, 2013) appears to be primarily related to the thickest crust, insofar that the Bouguer gravity anomaly is an indicator of crustal thickness (Judson, 1975; Hack, 1979; 1982), as the RMSD is maximized for the 100 km wavelength topographic filtering that we know to be consistent with crustal thickness variations. Late Cenozoic dynamic topography (Forte *et al.*, 2007; Moucha *et al.*, 2008; Rowley *et al.*, 2013; Moucha & Ruetenik, 2017) as well as post-orogenic isostatic and flexural isostatic processes (Pazzaglia & Gardner, 1994; 2000; Hawman *et al.*, 2012; Wagner *et al.*, 2012) likely play a secondary, but important role in divide evolution. Other, less well-understood processes such as residual effects from Eocene volcanism (Schmandt & Lin, 2014) and lithospheric foundering (Biryol *et al.*, 2016) may also be contributing factors.

The underlying causes for why the thick crustal root seems to be situated mostly under the Blue Ridge and the Appalachian foreland, rather than in the Piedmont which represents the former hinterland of the range is not clear, but probably is related to post-orogenic rifting, crustal

23

thinning, and subsequent opening of the Atlantic Ocean. Nonetheless, the late Mesozoic-Cenozoic post-orogenic Appalachians have had most isostatic support in the part of the orogen that was lowest-standing during the Paleozoic-early Mesozoic constructional phase. This has resulted in an inversion of the topography, and exhumation of the foreland by Atlantic slope drainages sometime after the late Triassic and early Jurassic (Judson, 1975). Presumably the westward march of the drainage divide since that time has been influenced by density or compositional changes in the crustal structure (Fischer, 2002), flexural isostatic (Pazzaglia & Gardner, 1994; 2000), and dynamic mantle support (Moucha *et al.*, 2008).

At lithospheric thickness wavelengths, the redistribution of surface loads due to erosion and deposition of sediments cause flexural isostatic bending of the margin (Pazzaglia & Gardner, 1994; 2000; Moucha & Ruetenik, 2017). The result is an amplification of the Atlantic slope eastward tilt, with a hinge balanced on the Fall Zone that separates subsidence beneath the Coastal Plain and uplift of the Piedmont. Farther west, the flexural models predict a small, but significant peripheral bulge of several tens of meters that falls mostly west of the current drainage divide, particularly in the central Appalachians (Pazzaglia & Gardner, 1994; 2000; Moucha & Ruetenik, 2017; Fig. 11). This flexural isostatic deformation, driven by the deposition of large volumes of sediment in the Baltimore Canyon trough in the Miocene (Fig. 11, inset), has contributed to the uplift of the foreland, west of the present divide. The westward stepping of the synthetic divide (Fig. 6) across several physiographic provinces underlain by bedrock of diverse resistance (Meyerhoff, 1972; Hack, 1975; 1979; 1982) is explained in part by the flexural peripheral bulge and its co-location with the crustal root. The redistribution of surface loads and growth of the peripheral bulge to the west of the actual divide feeds back into how the divide migrates, that is, a positive feedback that leads to more divide migration, higher sediment fluxes, and thus further flexural deformation. Alternatively, if the peripheral bulge uplift is not focused to the west of the actual divide but rather co-located or east of the divide, a negative feedback pins the divide migration, leading to reduced divide migration and lower sediment fluxes. Piecemeal foundering of the lower lithosphere in a post-orogenic setting (Biryol *et al.*, 2016) could conceivably contribute to changes in lithospheric loads and effective elastic thickness, both expressed as long-wavelength flexural effects that would also impact the location of the divide.

24

Specific to our study region, a recent tomographic model of the entire Unites States using the EarthScope transportable array dataset identifies one of the largest anomalies in slower S- and P-wave velocities as lying beneath the central Appalachians (central Appalachian anomaly, CAA, Fig. 11) at a depth of ~200 km (Schmandt & Lin, 2014). At this depth, the anomaly is equal in magnitude and area to those imaged beneath the active margin of the western United States. At more shallow lithospheric depths, the CAA is reduced, if present at all. Presumably, the CAA is a zone of warm, buoyant asthenospheric mantle that may be responsible for the small-volume Eocene magmatism present in this region (Mazza *et al.*, 2014), that continues to have a dynamic expression at the surface.

Active crustal deformation across the CAA is indicated by the warping of the mid-Pliocene Orangeburg scarp geomorphic marker (Rowley *et al.*, 2013, Fig. 11). The Rowley *et al.* (2013) study similarly models anomalously warm and buoyant asthenospheric mantle rising beneath the central Appalachians as part of a westward directed return flow driven by foundering of the Farallon slab. We note that the largest deviation values coincide with the JRN gap and the CAA (Fig. 7C, 11), just west of the zone of maximum crustal uplift in the Rowley *et al.* (2013) model (Fig. 11). We suggest that crustal deformation driven by dynamic mantle flow is responsible for adding several tens of meters to the already isostatically and flexurally supported topography (Moucha & Ruetenik, 2017), a feature revealed in our 100- and 150-km filtered results (Fig. 6B), generating the potential for continued westward migration of the divide.

There is good sedimentologic (Scholle *et al.*, 1977; 1980; Poag, 1985, 1992; Poag & Sevon, 1989), thermochronologic (Spotila *et al.*, 2004; Naeser *et al.*, 1999; 2004; 2006, 2016), and geomorphic (Harbor *et al.*, 2005; Gunnell & Harbor, 2010; Prince *et al.*, 2010, 2011) evidence that the Appalachian continental divide migrates by episodic, major river captures. For example, the heavy mineral analysis of the COST-B2 well that penetrated the Baltimore Canyon Trough basin reveals four distinct heavy mineral suites from the Jurassic through the Pleistocene (Smith, 1980). The youngest of these suites is characterized by relatively unweathered pyroxene and amphiboles, and notably, a high percentage of rounded zircon, sphene, and staurolite that contrasts sharply with the stratigraphically older suites that are characterized by tourmaline, garnet, epidote, and chlorite (Smith, 1980). A reasonable interpretation is that the youngest suite, representing sediments of Miocene to Pleistocene in age, has a significant Ridge and Valley provenance that has liberated reworked heavy minerals from foreland basin sandstones, mixed with relatively unweathered glacial material, whereas sediments older than Miocene are dominated by heavy minerals with a Piedmont and Blue Ridge provenance. In this context, the huge increase in sediment flux to the Baltimore Canyon Trough in the Miocene (Fig. 11, inset), typically interpreted as a change in rock uplift or climate (Pazzaglia & Brandon, 1996), might more simply reflect a large westward jump in the continental divide, and the subsequent rapid incision of the newly acquired Atlantic slope landscape (Harbor *et al.*, 2005; Gunnell & Harbor, 2010). There are related geomorphic and sedimentologic data to suggest that the Miocene jump in the Appalachian divide started first in central Pennsylvania, and migrated southwest to its current location in western Virginia and the JRN gap (Pazzaglia, 1993).

In contrast, the James River has only recently (Pleistocene) worked its way west of the Blue Ridge into the Ridge and Valley (Harbor *et al.*, 2005) and the Roanoke River is still attempting to breach the Blue Ridge in western Virginia (Prince *et al.*, 2011). In the headwaters of the Roanoke River, there are examples of captures that have almost certainly occurred in the last million years. This conclusion is supported by the non-uniform distribution of erosion rates measured across the drainage divides, and contrasting headwater stream χ values (Portenga *et al.*, 2013; Figs. 8B, 9B, 10). As a result, we interpret the migration behavior of the Appalachian divide to primarily reflect exogenic forcings, but note the role of autogenic processes in introducing significant lag times to drainage capture and erosional response. The dynamic topographic forcing of rock uplift in the Appalachian foreland referenced here sets up a long-wavelength topographic gradient that can be exploited by any number of Atlantic slope rivers in pushing the continental divide west. We conclude that it is likely autogenic processes and stochastic events such as a landslides, sapping though a particularly soft rock, or debris dam in a headwater stream that determine which drainages are first to accomplish a drainage capture and push the divide to a new location.

7.3 The length scale of exogenic forcing, time lags of continental divide migration, and sediment delivery to basins

For both the Gibraltar Arc plate boundary and Appalachian plate interior setting, we note that the largest deviations in the location of the synthetic and actual divides and in χ values occur when topography is filtered at long wavelengths. We find, for example, that topography filtered at the short 50 km wavelengths essentially mimics the actual topography, and that at this scale, drainage divides are either stable or moving only back and forth, driven by autogenic and probably stochastic geomorphic processes acting on the hillslopes and channel heads. In contrast, at the 100- and 150-km scale of topographic filtering, there is good general co-location of the continental divide to known or modeled lithospheric scale exogenic processes or structure including Moho depth, lithospheric foundering, asthenospheric mantle circulation (dynamic topography), and flexural isostasy (Moucha & Ruetenik, 2017). Major watersheds draining both the active and decay-phase orogens studied here are organized by topographic gradients that are expressed in long-wavelength low-pass filtered topography ($\lambda \geq 100$ km). In contrast, topographic gradients measured over filtered wavelengths < 100 km are set by local crustal structures and rock type. Rivers are relatively insensitive to these local topographic gradients, hence the common presence of gorges where a river traverses a particularly resistant bedrock or encounters a rising structure such as a growing fold. Conversely, rivers are very sensitive to the long-wavelength tilting of a landscape and the continental divide shifts to always follow the regionally highest-standing topography.

Although not addressed directly in our study, the distribution of erosion rate data with the deviation measurements (Fig. 8) provides some insight into the time lag between the exogenic forcing and geomorphic responses that move divides, ultimately impacting the delivery of sediment from continental watersheds to sedimentary basins (Forzoni *et al.*, 2014), river incision (Yanites *et al.*, 2013), and topography at the landscape scale (Yang *et al.*, 2015). For the Gibraltar Arc, high erosion rates generally coincide with high deviation values (Fig. 8A), an observation consistent with short erosional response times to the exogenic forcing. Here, the active tectonic setting, steep hillslopes, and rivers with a short and steep run to base-level all contribute to the inferred short geomorphic response times in this setting. In contrast, the erosion rates in the Appalachians do not clearly mimic the local deviation values and in fact, could be argued to be anti-correlated, although there is much scatter in the data (Fig. 8B). It is possible that in the

27

decaying orogen, intraplate setting of the Appalachians, that the more gentle slopes and low overall erosion rates, which are closely related to the rates of soil production and hillslope creep, permit a wide range of erosion rates to persist in the regions where the actual divide has already adjusted to the synthetic divide. In this setting, the landscape remains in a state of local disequilibrium for a long period of time as drainage reorganization perturbations resonate through the fluvial and hillslope systems. Similarly, in regions where there is a large local deviation, like the JRN gap, the erosion rates are slow precisely because the actual divide has yet to migrate to the location predicted by the synthetic divide and base level has not yet fallen. These results reinforce the notion that stratigraphic packages deposited in basins in both tectonically active and passive margins primarily encode exogenic forcings, whereby divide migration and change in drainage basin size result in, for example, significant progradation of a shoreline, aggradation and fan growth, or coarsening-up of a clastic sequence (Leeder et al., 1998; Clift, 2006).

Aspects of these observations and interpretations have been reported by others. For example, the Great Dividing Range of eastern Australia is a post-rift great escarpment that is slowly migrating westward at a rate of ~3-30 m/Ma (Seidl *et al.*, 1996; Heimsath *et al.*, 2006) on a passive margin, intraplate setting with some similarities to the Appalachians (Spotila *et al.*, 2004). Here, the Bouguer gravity anomaly is used to indicate crustal thickness and the area where topography is likely being impacted at a long-wavelength by isostatic support. It is noted that in this setting, the continental divide mostly follows the highest-standing isostatically supported topography. However, for about 20% of the of the length of the range, the divide separates from the gravity low and high-standing topography and shifts to the east. In this same region, there is geomorphic evidence for recent drainage captures expanding inland drainage systems, i.e., eastward divide migration (Young, 1989). The separation of the divide here from the long-wavelength high-standing topography has been associated with the Lake Galilee lineament, an additional substantial lithospheric scale feature that localizes the divide (Harrington *et al.*, 1982; Young, 1989). Müller *et al.* (2016) demonstrated rejuvenated Cenozoic dynamic topography in northeastern Australia associated with the gradual NNE migration of the Australian plate over the edge of the large Pacific mantle upwelling that is potentially associated

28

with ongoing eastward divide migration along the Australian passive margin.

With many features in common to the Gibraltar Arc, the long-wavelength, or regional-scale, topography of the tectonically active Central Apennines of the Italian Peninsula is argued to be dynamically supported, and migrating eastward with continued rollback of the Adriatic slab (D'Agostino *et al.*, 2001). The Apennine continental divide aligns well with the high-standing long-wavelength topography of the peninsula identified by D'Agostino *et al.* (2001) (i.e., where the synthetic divide would be located), but the actual and synthetic divides are mis-placed with respect to the axis of highest-standing peak elevations. East-flowing rivers carve deep gorges through the line of highest-standing peaks, an incision that is driven in part by headwater captures as the orogenic divide shifts. The presence of the deep gorges and overlap of the actual and synthetic divides is consistent with the notion that the major geomorphic gradient of the landscape produced by the long-wavelength dynamically supported topography is responsible for driving drainage network reorganization. In the case of the Central Apennines, the reorganization is rapid enough that there is little deviation between the actual and synthetic divides. In essence, the topographic gradient established by differential surface uplift is strong enough that the east-flowing rivers were able to carve deep gorges enabling the headwaters to migrate beyond the high short-wavelength peaks of the Apennines so that the divides are overlapping.

8.0 Conclusions

Our observations in the plate boundary setting of the Gibraltar Arc and intraplate setting of the Appalachians, in comparison to similar studies in Australia (Young, 1989), Italy (D'Agostino *et al.*, 2001), and the western US (Wegmann *et al.*, 2007) illustrate the impact of exogenic, long-wavelength crustal deformation on continental divide migration. Major rivers flow in the direction of the regional gradients of the lithosphere, which are tectonically, isostatically, or dynamically influenced, even if those regional gradients are gentle. In many landscapes, these regional gradients are clearly reflected in the topography. In other cases, local

29

topographic highs or lows can be superimposed on the regional gradients, but the local features tend to have little effect on the overall drainage topology. Continental divides are often separated from the highest-standing peaks and local topography and nucleate instead on the crests of the long-wavelength topography as synthesized using a low-pass filter.

Continental divides migrate in the direction of the higher-standing synthetic divide set by lithospheric scale structures and processes. Autogenic processes and feedbacks on divide migration cause the process to be unsteady and occur through pulses of drainage capture and drainage network reorganization that may have record in sedimentological, geomorphic, or denudation rate data. Our analysis, utilizing isolated long-wavelength filtered topography and the χ transformation calculation, provides a novel framework for predicting the direction of divide movement, as well as an estimate of the ultimate divide location. The direction of predicted or ongoing divide migration may be a tool for interpreting various models of geodynamic evolution of geologic settings, sediment routing to basins, and the relative controls of various geophysical anomalies on the expression of surface topography.

9.0 Acknowledgements

We thank David Anastasio, Peter Zeitler, and two anonymous reviewers for their insightful comments on an early draft of this manuscript. Further improvement was supported by Nathan Lyons and two anonymous reviewers, whom we thank for their comments and suggestions. A. J. M. acknowledges support by the National Science Foundation Graduate Research Fellowship under Grant No. 145068.

References

ANDERSON, A. L. (1947) Drainage diversion in the northern Rocky Mountains of east-central Idaho. *Journal of Geology*, 55, 61–75.

AZAÑÓN, J. M., GALVE, J. P., PÉREZ-PEÑA, J. V. & ROLDAN, F. J. (2015) Relief and drainage evolution during exhumation of the Sierra Nevada (SE Spain): Is denudation keeping pace with uplift? *Tectonophysics*, 663, doi:10.1016/j.tecto.2015.06.015.

AZAÑÓN, J. M., PÉREZ-PEÑA, J. V., GIACONIA, F., BOOTH-REA, G., MARTÍNEZ-MARTÍNEZ, J. M. & RODRÍGUEZ-PECES, M. J. (2012) Active tectonics in the central

30

and eastern Betic Cordillera through morphotectonic analysis: the case of Sierra Nevada and Sierra Alhamilla. *Journal of Iberian Geology*, 38, 225–238.

AZAÑÓN, J. M., TUCCIMEI, P., AZOR, A., SÁNCHEZ-ALMAZO, I. M., ALONSO-ZARZA, A. M., SOLIGO, M. & PÉREZ-PEÑA, J. V. (2006) Calcrete features and age estimates from U/Th dating: implications for the analysis of Quaternary erosion rates in the northern limb of the Sierra Nevada range (Betic Cordillera, southeast Spain. In: *Paleoenvironmental record and applications of calcretes and palustrine Carbonates,* (Ed. by A. M. Alonso-Zarza & L. H. Tanner), *Geology Society of America Special Paper* 416, 223–239.

BEAUMONT, C., FULLSACK, P. & HAMILTON, J. (1992) Erosional control of active compressional orogens. In: *Thrust Tectonics,* (Ed. by K. R. McClay), 1–18. Chapman and Hall.

BELLIN, N., VANACKER, V. & KUBIK, P. W. (2014) Denudation rates and tectonic geomorphology of the Spanish Betic Cordillera. *Earth and Planetary Science Letters,* 390, 19–30. doi: 10.1016/j.epsl.2013.12.045.

BERTI, C., ANASTASIO, D. J., PAZZAGLIA, F. J., BROCARD, G. Y., MOODIE, A., PARES, J. M., CENIEH, P. S. A. & SOTO, J. I. (2014) Drainage network reorganization and divide migration in response to active tectonics in the Betic Range, Spain: *Geological Society of America Abstracts with Programs*, 46 (6).

BEZADA, M. J., HUMPHREYS, E. D., DAVILA, J. M., CARBONELL, R., HARNAFI, M., PALOMERAS, I. & LEVANDER, A. (2014) Piecewise delamination of Moroccan lithosphere from beneath the Atlas Mountains. *Geochemistry, Geophysics, Geosystems,* doi: 10.1002/2013GC005059.

BEZADA, M. J., HUMPHREYS, E. D., TOOMEY, D. R., HARNAFI, M., DAVILA, J. M. & GALLART, J. (2013) Evidence for slab rollback in westernmost Mediterranean from improved upper mantle imaging. *Earth and Planetrary Science Letters*, 368, 51–60.

BIRYOL, C. B., WAGNER, L. S., FISCHER, K. M. & HAWMAN, R. B. (2016) Relationship between observed upper mantle structures and recent tectonic activity across the Southeastern United States. *Journal of Geophysical Research: Solid Earth*, 121,

31

doi:10.1002/2015JB012698.

BLACK, B. A., PERRON, J. T., HEMINGWAY, D., BAILEY, E., NIMMO, F. & ZEBKER, H. (2017) Global drainage patterns and the origins of topographic relief on Earth, Mars, and Titan. *Science,* 356, 727–731. doi: 10.1126/science.aag0171.

BOSSU, C. M., BEAULIEU, J. M., CAES, P. A. & NEAR, T. J. (2013) Explicit tests of palaeodrainage connections of southeastern North America and the historical biogeography of Orangethroat Darters (Percidae: Etheostoma: Ceasia). *Molecular Ecology,* 22, 5397–5417. doi: 10.1111/mec.12485.

CALVACHE, M. & VISERAS, C. (1997) Long-term control mechanisms of stream piracy processes in southeast Spain. *Earth Surface Processes and Landforms*, 22, 93–105.

CALVERT, A., SANDVOL, E. SEBER, D., BARAZANGI, M., ROECKER, S., MOURABIT, T., VIDAL, F., ALGUACIL, G. & JABOUR, N. (2000) Geodynamic evolution of the lithosphere and upper mantle beneath the Alboran region of the western Mediterranean: Constraints from travel time tomography. *Journal of Geophysical Research,* 105 (B5), doi: 10.1029/2000JB900024.

CIOLKOSZ, E. J., CARTER, B. J., HOOVER, M. T., CRONCE, R. C., WALTMAN, W. J. & DOBOS, R. R. (1990) Genesis of soils and landscapes in the Ridge and Valley province of central Pennsylvania, In: *Soils and Geomorphology,* (Ed. by L. D. McFadden & P. L. K. Knuepfer), 3 (3–4), 245–262.

CLIFT, P. D. (2006) Controls on the erosion of Cenozoic Asia and the flux of clastic sediment to the ocean. *Earth and Planetary Science Letters*, 241, 571–580.

CLARK, S. J. P. & DEMPSTER, T. J. (2009) The record of tectonic denudation and erosion in an emerging orogen: an apatite fission-track study of the Sierra Nevada, southern Spain. *Journal of the Geological Society*, 166, 87–100.

CROSBY, B. T. & WHIPPLE, K. X. (2006) Knickpoint initiation and distribution within fluvial networks: 236 waterfalls in the Waipaoa River, North Island, New Zealand. *Geomorphology*, 82, 16–38.

D'AGOSTINO, N., JACKSON, J. A., DRAMIS, F. & FUNICIELLO, R. (2001) Interactions between mantle upwelling, drainage evolution and active normal faulting: an example from the central Apennines (Italy). *Geophysical Journal International*, 147 (2), 475–497.

 32

doi: 10.1046/j.1365-246X.2001.00539.x.

DAVIS, W. M. (1903) The stream contest along the Blue Ridge. *Geographical Society of Philadelphia Bulletin*, 3, 213–244.

FAILL, R. T. (1997a) A geologic history of the north-central Appalachians; Part 1, Orogenesis from the Mesoproterozoic through the Taconic Orogeny. *American Journal of Science,* 297, 551–619.

FAILL, R. T. (1997b) A geologic history of the north-central Appalachians; Part 2, The Appalachian Basin from the Silurian through the Carboniferous. *American Journal of Science*, 297, 729–761.

FISCHER, K. M. (2002) Waning buoyancy in the crustal roots of old mountains. *Nature*, 417 (6892), 933–936. doi: 10.1038/nature00855.

FLAMENT, N., GURNIS, M., AND MULLER, R. D. (2013) A review of observations and models of dynamic topography. *Lithosphere*, 5, 189–210.

FORTE, A. M., MITROVICA, J. X., MOUCHA, R., SIMMONS, N. A. & GRAND, S. P. (2007) Descent of the ancient Farallon slab drives localized mantle flow below the New Madrid seismic zone. *Geophysical Research Letters*, 34 (4), ISSN 0094-8276. doi: 10.1029/2006GL027895.

FORTE A. M., PELTIER W. R., DZIEWONSKI A. M. & WOODWARD R. L. (1993) Dynamic surface topography: A new interpretation based upon mantle flow models derived from seismic tomography. *Geophysical Research Letters*, 20 (3), 225–228, doi:10.1029/93GL00249.

FORZONI, A., STORMS, J. E. A., WHITTAKER, A. C. & de JAGER G. (2014) Delayed delivery from the sediment factory: modeling the impact of catchment response time to tectonics on sediment flux and fluvio-deltaic stratigraphy. *Earth Surface Processes and Landforms*, 39, 689–704.

FULLEA, J., FERNÀNDEZ, M., AFONSO, J., VERGÀS, J. & ZEYEN, H. (2010) The structure and evolution of the lithosphere-asthenosphere boundary beneath the Atlantic-Mediterranean Transition Region. *Lithos,* 120 (1–2), 74–95. ISSN 00244937. doi: 10.1016/j.lithos.2010.03.003.

GALLEN, S. F., WEGMANN, K. W. & BOHNENSTIEH, D. R. (2013) Miocene rejuvenation of

33

topographic relief in the southern Appalachians. *GSA Today*, 23 (2), 4–10. ISSN 10525173. doi: 10.1130/GSATG163A.1.

GARCIA-CASTELLANOS, D. & VILLASEÑOR, A. (2011) Messinian salinity crisis regulated by competing tectonics and erosion at the Gibraltar Arc. *Nature*, 480 (7377), 359–363. ISSN 0028-0836, doi: 10.1038/nature10651.

GARCÍA, A. F., ZHU, Z., KU, T. L., CHADWICK, O. A. & MONTERO, J. C. (2004) An incision wave in the geologic record, Alpujarran Corridor, southern Spain (Almeria). *Geomorphology*, 60, 37–72.

GARCÍA, A. F., ZHU, Z., KU, T. L., SANZ DE GALDEANO, C., CHADWICK, O. A. & CHACON MONTERO, J. (2003) Tectonically driven landscape development within the eastern Alpujarran Corridor, Betic Cordillera, E Spain (Almería). *Geomorphology*, 50, 83–110.

GILBERT, G. K. (1877) *Report on the Geology of the Henry Mountains.* US Geographical and Geological Survey of the Rocky Mountain Region, Department of the Interior, 2nd edition.

GUNNELL, Y. & HARBOR, D. J. (2010) Butte detachment: How pre-rift geological structure and drainage integration drive escarpment evolution at rifted continental margins. *Earth Surface Processes and Landforms*, 35, 1373–1385.

GURNIS M., MITROVICA J. X., RITSEMA J. & VAN HEIJST H.-J. (2000) Constraining mantle density structure using geological evidence of surface uplift rates: The case of the African superplume. *Geochemistry, Geophysics, Geosystems*, 1 (7), 1–31, doi:10.1029/1999GC000035.

HACK, J. T. (1975) Dynamic equilibrium and landscape evolution. In: *Theories of landform development*, (Ed. by W. N. Melhorn & R. C. Flemal), 87–102. Publications in Geomorphology, State University of New York, Binghamton, N.Y.

HACK, J. T. (1979) Rock control and tectonism: their importance in shaping the Appalachian highlands. *U. S. Geological Survey Professional Paper*. 1126-B, B1-B17.

HACK, J. T. (1982) Physiographic divisions and differential uplift in the Piedmont and Blue Ridge. *U. S. Geological Survey Professional Paper*. 1265.

34

HAJEK, E. A. & STRAUB, K. M. (2017) Autogenic sedimentation in clastic stratigraphy. *Annual Review of Earth and Planetary Sciences,* 45.

HARBOR, D., BACASTOW, A., HEATH, A. & ROGERS, J. (2005) Capturing the variable knickpoint retreat in the central Appalachians, USA. *Geografia Fisica e Dinammica Quaternaria,* 28, 23–36.

HARKINS, N., KIRBY, E., HEIMSATH, A., ROBINSON, R. & REISER, U. (2007) Transient fluvial incision in the headwaters of the Yellow River, northeastern Tibet, China. *Journal of Geophysical Research: Earth Surface,* 112, F03S04, doi:10.1029/2006JF000570.

HARRINGTON, H. J., SIMPSON, C. J. & MOORE, R. F. (1982) Analysis of continental structures using a digital terrain model (DTM) of Australia. *BMR Journal of Australian Geology* & *Geophysics,* 7, 68–72.

HARVEY, A. M. & WELLS, S. G. (1987) Response of Quaternary fluvial systems to differential epeirogenic uplift: Aguas and Feos river systems, southeast Spain. *Geology,* 15, 689–693.

HAWMAN, R. B., KHALIFA, M. O. & BAKER, M. S. (2012) Isostatic compensation for a portion of the Southern Appalachians: Evidence from a reconnaissance study using wide-angle, three-component seismic soundings. *Geological Society of America Bulletin,* 124 (3–4), 291–317. doi: 10.1130/B30464.1.

HEIMSATH, A. M., CHAPPELL, J., FINKEL, R. C., FIFIELD, K. & ALIMANOVIC, A. (2006) Escarpment erosion and landscape evolution in southeast Australia. In: *Tectonics, Climate, and Landscape Evolution*, (Ed. by S. D. Willett, N. Hovius, M. T. Brandon & D. M. Fisher), *Geological Society of America Special Paper 398,* Penrose Conference Series. 173–190, doi: 10.1130/2006.2398(10).

HOWARD, A. D. (1994) A detachment-limited model of drainage basin evolution, *Water Resources Research*, 30 (7), 2261–2285.

HOWARD, A. D. & KERBY, G. (1983) Channel changes in badlands, *Geological Society of America Bulletin*, 94, 739–752.

JOHNSON, C. (1997) Resolving denudational histories in orogenic belts with apatite fission-track thermochronology and structural data: An example from southern Spain. *Geology,* 25 (7).

JOHNSON, D. W. (1907) Drainage modifications in the Tallulah district. *Boston Society of*

35

Natural History Proceedings, 23, 211–248.

JOHNSON, D. W. (1931) Stream sculpture on the Atlantic slope: New York. *Columbia University Press*.

JUDSON, S. (1975) Evolution of Appalachian topography. In: *Theories of landform development*, (Ed. by W. N. Melhorn & R. C. Fleman), 29–44. Publications in Geomorphology, State University of New York, Binghamton, N.Y.

KARLSTROM, K. E., COBLENZ, D., DUEKER, K., OUIMET, W., KIRBY, E., VAN WIJK, J., SCHMANDT, B., KELLEY, S., LAZEAR, G., CROSSEY, L. J., CROW, R., ASLAN, A., DARLING, A., ASTER, R., MACCARTHY, J., HANSEN, S. M., STACHNIK, J., STOCKLI, D. F., GARCIA, R. V., HOFFMAN, M., McKEON, R., FELDMAN, J., HEIZLER, M., DONAHUE, M. S. & THE CREST WORKING GROUP (2012) Mantle-driven dynamic uplift of the Rocky Mountains and Colorado Plateau and its surface response: Toward a unified concept. *Lithosphere*, 4, 3–22.

KUCKS, R. P. (1999) Bouguer gravity anomaly data grid for the conterminous US. Online at http://mrdata.usgs.gov/gravity/bouguer/.

LASKE, G., MASTERS., G., MA, Z. & PASYANOS, M. (2013) Update on CRUST1.0 - A 1-degree Global Model of Earth's Crust. *Geophysical Research Abstracts*, 15, Abstract EGU2013-2658.

LEEDER, M. R., HARRIS, T. & KIRKBY, M. J. (1998) Sediment supply and climate change: implications for basin stratigraphy. *Basin Research*, 10, 7–18.

LINK, P. K. & HODGES, M. K. V. (2011) The Neogene drainage history of south-central Idaho. In: *Geologic Field Trips to the Basin and Range, Rocky Mountains, Snake River Plain and Terranes of the U.S. Cordillera*, (Ed. by J. Lee & J. P. Evans), Geological Society of America Field Guide 21, 103–123.

LIS MANCILLA, F. d., STICH, D., BERROCOSO, M., MARTÍN, R., MORALES, J., FERNANDEZ-ROS, A., PÁEZ, R. & PÉREZ-PEÑA, A. (2013) Delamination in the Betic Range: Deep structure, seismicity, and GPS motion. *Geology*, 41 (3), 307–310. ISSN 0091-7613, 1943-2682. doi: 10.1130/G33733.1.

LONERGAN, L. (1993) Timing and kinematics of deformation in the Malaguide Complex, internal zone of the Betic Cordillera, southeast Spain. *Tectonics*, 12 (2), 460–476. doi:

36

10.1029/92TC02507.

LONERGAN, L. & MANGE-RAJETZKY, M. (1994) Evidence for Internal Zone unroofing from foreland basin sediments, Betic Cordillera, SE Spain. *Journal of the Geological Society*, 151, DOI: 10.1144/gsjgs.151.3.0515.

LONERGAN, L. & WHITE, N. (1997) Origin of the Betic-Rif mountain belt. *Tectonics*, 16 (3), 504–522. doi: 10.1029/96TC03937.

MAHER, E. & HARVEY, A. M. (2008) Fluvial system response to tectonically induced base-level change during the late Quaternary: The Rio Alias southeast Spain. *Geomorphology*, 100, 180–192.

MATHER, A. E. (2000) Adjustment of a drainage network to capture induced base-level change: an example from the Sorbas Basin, SE Spain. *Geomorphology*, 34, 271–289.

MATMON, A. S., BIERMAN, P., LARSEN, J., SOUTHWORTH, S., PAVICH, M., FINKEL, R. & CAFFEE, M. (2003) Erosion of an ancient mountain range, the Great Smoky Mountains, North Carolina and Tennessee. *American Journal of Science*, 303, 817–855.

MAZZA, S. E., GAZEL, E., JOHNSON, E. A., KUNK, M. J., McALEER, R., SPOTILA, J. A. & COLEMAN, D. S. (2014) Volcanoes of the passive margin: the youngest magmatic event in eastern North America. *Geology*, 42, 483–486.

McKEON, R. E., ZEITLER, P. K., PAZZAGLIA, F. J., IDLEMAN, B. D. & ENKELMANN, E. (2013) Decay of an old orogen: Inferences about Appalachian landscape evolution from low-temperature thermochronology. *Geological Society of America Bulletin*, 126 (1–2), 31–46. doi: 10.1130/B30808.1.

MEYERHOFF, H. A. (1972) Postorogenic development of the Appalachians. *Geological Society of America Bulletin*, 83, 1709–1728.

MEYERHOFF, H. A. & OLMSTED, E. W. (1936) The origins of Appalachian drainage. *American Journal of Science*, 32, 21–42.

MILLS, H. H. (2000) Apparent increasing rates of stream incision in the eastern United States during the late Cenozoic. *Geology*, 28 (10), 955–957.

MITROVICA J. X., BEAUMONT C. & JARVIS G. T. (1989) Tilting of continental interiors by the dynamical effects of subduction. *Tectonics*, 8 (5), 1079–1094. doi:10.1029/TC008i005p01079.

MOUCHA, R., FORTE, A. M., MITROVICA, J. X., ROWLEY, D. B., QUÉRÉ, S., SIMMONS, N. A. & GRAND, S. P. (2008) Dynamic topography and long-term sea-level variations: There is no such thing as a stable continental platform. *Earth and Planetary Science Letters*, 271 (1–4), 101–108. doi: 10.1016/j.epsl.2008.03.056.

MOUCHA, R. & RUETENIK, G. A. (2017) Interplay between dynamic topography and flexure along the U.S. Atlantic passive margin: Insights from landscape evolution modeling. *Global and Planetary Change*, 149, 72–78.

MÜLLER, R. D., FLAMENT, N., MATTHEWS, K. J., WILLIAMS, S. E. & GURNIS, M. (2016) Formation of Australian continental margin highlands driven by plate-mantle interaction. *Earth and Planetary Science Letters*, 441, 60–70.

NAESER, C. W., NAESER, N. D., NEWELL, W. L., SOUTHWORTH, S., EDWARDS, L. E. & WEEMS, R. E. (2016) Erosional and depositional history of the Atlantic passive margin as recorded in detrital zircon fission-track ages and lithic detritus in Atlantic Coastal Plain sediments. *American Journal of Science*, 316, 110–168.

NAESER, N. D., NAESER, C. W., MORGAN, B. A., III, SCHULTZ, A. P. & SOUTHWORTH, C. S. (1999) Paleozoic to Recent cooling history of the Blue Ridge province, Virginia, North Carolina, and Tennessee, from apatite and zircon fission-track analysis. *Geological Society of America Abstracts with Programs*, 31 (7), A-117.

NAESER, N. D., NAESER, C. W., NEWELL, W. L., SOUTHWORTH, S., WEEMS, R. E. & EDWARDS, L. E. (2006) Provenance studies in the Atlantic Coastal Plain: What fission-track ages of detrital zircons can tell us about the erosion history of the Appalachians. *Geological Society of America Abstracts with Programs*, 38 (7), 503.

NAESER, N. D., NAESER, C. W., SOUTHWORTH, C. S., MORGAN, B. A., III & SCHULTZ, A. P. (2004) Paleozoic to Recent tectonic and denudation history of rocks in the Blue Ridge province, central and southern Appalachians—evidence from fission-track thermochronology. *Geological Society of America Abstracts with Programs,* 36 (2), 114.

OLIVER, J., COOK, F. & BROWN, L. (1983) COCORP and continental crust. *Journal of Geophysical Research,* 88, 3329–3347.

PALOMERAS, I., THURNER, S., LEVANDER, A., LIU, K., VILLASENOR, A.,

38

CARBONELL, R. & HARNAFI, M. (2014) Finite-frequency Rayleigh wave tomography of the western Mediterranean: Mapping its lithospheric structure. *Geochemistry, Geophysics, Geosystems*, 15, 140–160, doi:10.1002/2013GC004861.

PAVICH, M. J. (1989) Regolith residence time and the concept of surface age of the Piedmont “peneplain”. In: *Appalachian Geomorphology*, (Ed. by T. W. Gardner & W. D. Sevon), 2 (1–3), 181–196.

PAZZAGLIA, F. J. (1993) Stratigraphy, petrography, and correlation of late Cenozoic middle Atlantic Coastal Plain deposits: Implications for late-stage passive margin geologic evolution. *Geological Society of America Bulletin*, 105, 1617–1634.

PAZZAGLIA, F. J. & BRANDON, M. T. (1996) Macrogeomorphic evolution of the post-Triassic Appalachian mountains determined by deconvolution of the offshore basin sedimentary record. *Basin Research*, 8 (3), 255–278. doi: 10.1046/j.1365-2117.1996.00274.x.

PAZZAGLIA, F. J., CARTER, M., BERTI, C., COUNTS, R., HANCOCK, G., HARBOR, D., HARRISON, R., HELLER, M., MAHAN, S., MALENDA, H., McKEON, R., NELSON, M., PRINCE, P., RITTENOUR, T., SPOTILA, J. & WHITTECAR, R. (2015) Geomorphology, active tectonics, and landscape evolution in the mid-Atlantic region. In: *Tripping from the Fall Line: Field Excursions for the GSA Annual Meeting, Baltimore, 2015*, (Ed. by D. K. Brezinski, J. P. Halka & R. A. Ortt Jr.), Geological Society of America Field Guide 40, 109–169, doi:10.1130/2015.0040(06).

PAZZAGLIA, F. J. & GARDNER, T. W. (1994) Late Cenozoic flexural deformation of the middle U. S. Atlantic passive margin. *Journal of Geophysical Research*, 99 (B6), 12,143–12,157.

PAZZAGLIA, F. J. & GARDNER, T. W. (2000) Late Cenozoic landscape evolution of the US Atlantic passive margin: insights into a North American Great Escarpment. In: *Geomorphology and Global Tectonics*, (Ed. by M. A. Summerfield), 284–302. Wiley Interscience, Chirchester.

PÉREZ-PEÑA, J. V., AZAÑÓN, J. M., AZOR, A., TUCCIMEI, P., DELLA SETA, M. & SOLIGO, M. (2009) Quaternary landscape evolution and erosion rates for an intramontane Neogene basin (Guadix-Baza basin, SE Spain). *Geomorphology*, 106 (3–4), 206–218. doi: 10.1016/j.geomorph.2008.10.018.

PERRON, J. T., DIETRICH, W. E. & KIRCHNER, J. W. (2008) Controls on the spacing of first-order valleys. *Journal of Geophysical Research*, 113, F04016. doi:10.1029/2007JF000977.

PERRON, J. T., KIRCHNER, J. W. & DIETRICH, W. E. (2009) Formation of evenly spaced ridges and valleys. *Nature*, 460, 502–505.

PERRON, J. T. & ROYDEN, L. (2013) An integral approach to bedrock river profile analysis. *Earth Surface Processes and Landforms*, 38, 570–576.

PIERCE, K. L. & MORGAN, L. A. (1992) The track of the Yellowstone hot spot—volcanism, faulting and uplift. In: *Regional geology of eastern Idaho and western Wyoming*, (Ed. by P. K. Link, M. A. Kuntz & L. W. Platt), Geological Society of America Memoir, 179, 1–53.

PLATT, J. P., BEHR, W. M., JOHANESEN, K. & WILLIAMS, J. R. (2013) The Betic-Rif Arc and its Orogenic Hinterland: A Review. *Annual Review of Earth and Planetary Sciences*, 41 (1), 313–357. doi: 10.1146/annurev-earth-050212-123951.

POAG, C. W. (1985) Depositional history and reference section for central Baltimore Canyon trough. In: *Geologic Evolution of the United States Atlantic margin*, (Ed. by C. W. Poag), 217–263. New York, Van Nostrand Reinhold.

POAG, C. W. (1992) U.S. Middle Atlantic continental rise; provenance, dispersal, and deposition of Jurassic to Quaternary sediments. In: *Geologic evolution of Atlantic continental rises*, (Ed. by C. W. Poag & P. C. de Graciansky), 100–156. New York, Van Nostrand Reinhold.

POAG, C. W. & SEVON, W. D. (1989) A record of Appalachian denudation in postrift Mesozoic and Cenozoic sedimentary deposits of the U.S. Middle Atlantic continental margin. *Geomorphology*, 2, 119–157.

PORTENGA, E. W., BIERMAN, P. R., RIZZO, D. M. & ROOD, D. H. (2013) Low rates of bedrock outcrop erosion in the central Appalachian Mountains inferred from in situ 10Be. *Geological Society of America Bulletin*, 125 (1–2), 201–215. ISSN 0016-7606, 1943-2674. doi: 10.1130/B30559.1.

PRINCE, P. S., SPOTILA, J. A. & HENIKA, W. S. (2010) New physical evidence of the role of

40

stream capture in active retreat of the Blue Ridge escarpment, southern Appalachians. *Geomorphology*, 123 (3–4), 305–319. doi: 10.1016/j.geomorph.2010.07.023.

PRINCE, P. S., SPOTILA, J. A. & HENIKA, W. S. (2011) Stream capture as driver of transient landscape evolution in a tectonically quiescent setting. *Geology*, 39, 823–826.

REINHARDT, L. J., BISHOP, P., HOEY, T. B., DEMPSTER, T. J. & SANDERSON, D. C. W. (2007) Quantification of the transient response to base-level fall in a small mountain catchment: Sierra Nevada, southern Spain. *Journal of Geophysical Research*, 112 (F3). doi: 10.1029/2006JF000524.

REUSSER, L., BIERMAN, P., PAVICH, M., LARSEN, J. & FINKEL, R. (2006) An episode of rapid bedrock channel incision during the last glacial cycle, measured with 10Be. *American Journal of Science*, 306, 69–102.

REUSSER, L. J., BIERMAN, P. R., PAVICH, M. J., ZEN, E.-a., LARSEN, J. & FINKEL, R. (2004) Rapid Late Pleistocene incision of Atlantic passive-margin river gorges. *Science*, 305, 499–502.

REUTER, J. M. (2005) Erosion rates and pattern inferred from cosmogenic 10Be in the Susquehanna River basin: M. S. Thesis, Burlington, University of Vermont, 160 p.

ROERING, J. J., KIRCHNER, J. W. & DIETRICH, W. E. (1999) Evidence for nonlinear, diffusive sediment transport on hillslopes and implications for landscape morphology. *Water Resoures Research*, 35, 853–870.

ROSENBAUM, G., LISTER, G. S. & DUBOZ, C. (2002) Reconstruction of the tectonic evolution of the western Mediterranean since the Oligocene. In: *Reconstruction of the evolution of the Alpine-Himalayan orogen*, (Ed. by G. Rosenbaum & G. S. Lister), Journal of the Virtual Explorer, 8 (6). doi:10.3809/jvirtex.2002.00053.

ROWLEY, D. B., FORTE, A. M., MOUCHA, R., MITROVICA, J. X., SIMMONS, N. A. & GRAND, S. P. (2013) Dynamic Topography Change of the Eastern United States Since 3 Million Years Ago. *Science*, 340 (6140), 1560–1563. doi: 10.1126/science.1229180.

RUETENIK, G. A., MOUCHA, R. & HOKE, G. D. (2016) Landscape response to changes in dynamic topography. *Terra Nova*, 28, 289–296.

SANZ DE GALDEANO, C. & LOPEZ-GARRIDO, A. C. (1999) Nature and impact of the neotectonic deformation in the western Sierra Nevada (Spain). *Geomorphology*, 30, 259–

41

272.

SCHMANDT, B. & LIN, F-C. (2014) P and S wave tomography of the mantle beneath the United States. *Geophysical Research Letters*, 41, 6342–6349, doi:10.1002/2014GL061231.

SCHOLLE, P. A. (1977) Geological studies on the COST No. B-2 well, U.S. mid-Atlantic outer continental shelf area. *U.S. Geological Survey Circular* 750. 71 p.

SCHOLLE, P. A. (1980) Geological studies of the COST No. B-3 well, United States mid-Atlantic continental slope area. *U.S. Geological Survey Circular* 833. 130 p.

SCHULTE, L., JULIÀ, R., BURJACHS, F. & HILGERS, A. (2008) Middle Pleistocene to Holocene geochronology of the River Aguas terrace sequence (Iberian Peninsula): Fluvial response to Mediterranean environmental change. *Geomorphology,* 98, 13–33, doi:10.1016/j.geomorph.2007.03.018.

SCHWANGHART, W. & SCHERLER, D. (2014). TopoToolbox 2 – MATLAB-based software for topographic analysis and modeling in Earth surface sciences. *Earth Surface Dynamics*, 2, 1–7. doi: 10.5194/esurf-2-1-2014.

SEARS, J. W., HENDRIX, M. S., THOMAS, R. C. & FRITZ, W. J. (2009) Stratigraphic record of the Yellowstone hotspot track, Neogene Sixmile Creek Formation grabens, southwest Montana. *Journal of Volcanology and Geothermal Research*, 188, 250–259.

SEBER, D., BARAZANGI, M., IBENBRAHIM, A. & DEMNATI, A. (1996), Geophysical evidence for lithosphereic delamination beneath the Alboran Sea and Rif-Betic mountains. *Nature*, 379, 785–790.

SEIDL, M. A., WEISSEL, J. K. & PRATSON, L. F. (1996) The kinematics and pattern of escarpment retreat across the rifted continental margin of SE Australia. *Basin Research,* 8, 301–316. doi:10.1046/j.1365-2117.1996.00266x.

SHERIDAN, R. E. & GROW, J. A. (1988) The Atlantic continental margin. *U. S. Geological Society of America, The Geology of North America*. 1–2, 527.

SIMPSON, R. W., HILDENBRAND, T. G., GODSON, R. H. & KANE, M. F. (1987) Digital colored Bouguer gravity, free-air gravity, station location, and terrain maps for the conterminous united states. *Geophysical Investigations Map*: 2 sheets.

SIMPSON, R. W., JACHENS, R. C., BLAKELY, R. J. & SALTUS, R. W. (1986) A New

 42

Isostatic Residual Gravity Map of the Conterminous United States with a Discussion on the Significance of Isostatic Residual Anomalies. *Journal of Geophysical Research*, 91, B8:8348. doi:10.1029/JB091iB08p08348.

SMITH, R. V. (1980) Provenance of mid-Atlantic continental margin sediments from the COST B-2 test well. unpublished M.S. Thesis. 182 p. University of Delaware, Newark, DE.

SNYDER, N. P., WHIPPLE, K. X., TUCKER, G. E. & MERRITTS, D. J. (2000) Landscape response to tectonic forcing: digital elevation model analysis of stream profiles in the Mendocino triple junction region, northern California. *Geological Society of America Bulletin*, 112, 1250–1263.

SPAKMAN, W. & WORTEL, R. (2004) A tomographic view on western Mediterranean geodynamics. In: *The TRANSMED Atlas. The Mediterranean Region from Crust to Mantle*, (Ed. by W. Cavazza, F. Roure, W. Spakman, G. M. Stampfli & P. A. Ziegler), 31–52. Springer Berlin Heidelberg, Berlin, Heidelberg. ISBN 978-3-642-62355-4, 978-3-642-18919-7.

SPOTILA, J. A., BANK, G. C., REINERS, P. W., NAESER, C. W. & HENIKA, W. S. (2004) Origin of the Blue Ridge escarpment along the passive margin of eastern North America. *Basin Research*, 16, 41–63.

STOKES, M. (2008) Plio-Pleistocene drainage development in an inverted sedimentary basin: Vera basin, Betic Cordillera, SE Spain. *Geomorphology*, 100, 193–211.

STOKES, M. & MATHER, A. E. (2003) Tectonic origin and evolution of a transverse drainage: the Rio Almanzora, Betic Cordilleria, southeast Spain. *Geomorphology*, 50, 59–81.

STOKES, M., MATHER, A. E. & HARVEY, A. M. (2002) Quantification of river-capture-induced base-level changes and landscape development, Sorbas Basin, SE Spain: *Geological Society Special Publication* 191, 23–35.

THORNBURY, W. D. (1965) Regional geomorphology of the United States. 609 p. New York, John Wiley and Sons.

TUCKER, G. E. & HANCOCK, G. R. (2010) Modelling landscape evolution. *Earth Surface Processes and Landforms*, 35, 28–50.

VÁZQUEZ, M., JABALOY, A., BARBERO, L. & STUART, F. (2011) Deciphering tectonic and

 43

erosion-driven exhumation of the Nevado–Filábride Complex (Betic Cordillera, Southern Spain) by low temperature thermochronology. *Terra Nova*, 23, 257–263.

WAGNER, L. S., STEWART, K. & METCALF, K. (2012) Crustal-scale shortening structures beneath the Blue Ridge Mountains, North Carolina, USA. *Lithosphere*, 4 (3), 242–256. doi: 10.1130/L184.1.

WARD, D. J., SPOTILA, J. S., HANCOCK, G. S. & GALBRAITH, J. M. (2005) New constraints on the late Cenozoic incision history of the New River, Virginia. *Geomorphology*, 72, 54–72.

WEGMANN, K. W., ZUREK, B. D., REGALLA, C. A., BILARDELLO, D., WOLLENBERG, J. L., KOPCZYNSKI, S. E., ZIEMANN, J. M., HAIGHT, S. L., APGAR, J. D., ZHAO, C. & PAZZAGLIA, F. J. (2007) Position of the Snake River watershed divide as an indicator of geodynamic processes in the greater Yellowstone region, western North America. *Geosphere*. 3 (4), 272. doi: 10.1130/GES00083.1.

WEIJERMARS, R., ROEP, TH. B., VAN DEN EECKHOUT, B., POSTMA, G. & KLEVERLAAN K. (1985). Uplift history of a Betic fold nappe inferred from Neogene-Quaternary sedimentation and tectonics (in the Sierra Alhamilla and Almeria, Sorbas and Tabernas Basins of the Betic Cordilleras, SE Spain). *Geologie en Mijnbouw*, 64, 397–411.

WESSEL, P. & SMITH, W. H. F. (1991) Free software helps map and display data. *Eos, Transactions American Geophysical Union*, 72 (41), 441–441. doi: 10.1029/90EO00319.

WHIPPLE, K. X., DIBIASE, R. A., OUIMET, W. B. & FORTE, A. M. (2017a) Preservation or piracy: Diagnosing low-relief, high-elevation surface formation mechanisms. *Geology*, 45 (1). doi:10.1130/G38490.1

WHIPPLE, K. X., FORTE, S. M., DIBIASE, R. A., GASPARINI, N. M. & OUIMET, W. B. (2017b) Timescales of landscape response to divide migration and drainage capture: Implications for the role of divide mobility in landscape evolution. *Journal of Geophysical Research: Earth Surface*, 122, 248–273.

WHIPPLE, K. X. & TUCKER, G. E. (1999) Dynamics of the stream power river incision model: Implications for height limits of mountain ranges, landscape response timescales and

44

research needs. *Journal of Geophysical Research*, 104, 17,661–17,674.

WILLETT, S. D., McCOY, S. W., PERRON, J. T., GOREN, L. & CHEN, C. Y. (2014) Dynamic reorganization of river basins. *Science*, 343 (6175). doi:10.1126/science.1248765.

WILSON, J. T. (1966) Did the Atlantic Close and then Re-Open? *Nature*, 211, 676–681.

YANG, R., WILLETT, S. D. & GOREN, L. (2015) In situ low-relief landscape formation as a result of river network disruption. *Nature*, 520, 526–529.

YANITES, B. J., EHLERS, T. A., BECKER, J. K., SCHNELLMANN, M. & HEUBERGER, S. (2013) High magnitude and rapid incision from river capture: Rhine River, Switzerland. *Journal of Geophysical Research*, 118. doi: 10.1002/jgrf.20056.

YOUNG, R. W. (1989) Crustal constraints on the evolution of the continental divide of eastern Australia. *Geology,* 17 (6), 528. doi: 10.1130/0091-7613(1989)017<0528:CCOTEO>2.3.CO;2.

ZECK, H. P., MONIÈ, P., VILLA, I. M. & HANSEN, B. T. (1992) Very high rates of cooling and uplift in the Alpine belt of the Betic Cordilleras, southern Spain. *Geology*, 10, 79–83.

ZEITLER, P. K., KOONS, P. O., BISHOP, M. L., CHAMBERLAIN, C. P., CRAW, D., EDWARDS, M. A., HAMIDULLAH, S., JAN, M. Q., KHAN, M. A., KHATTAK, M. U. K., KIDD, W. S. F., MACKIE, R. L., MELTZER, A. S., PARK, S. K., PECHER, A., POAGE, M. A., SARKER, G., SCHNEIDER, D. A., SEEBER, L. & SHRODER, J. (2001a) Crustal Reworking at Nanga Parbat, Pakistan: Evidence for erosional focusing of crustal strain. *Tectonics*, 20, 712–728.

ZEITLER, P. K., MELTZER, A. S., KOONS, P., CRAW, D., HALLET, B., CHAMBERLAIN, C. P., KIDD, W., PARK, S., SEEBER, L., BISHOP, M. & SHRODER, J. (2001b) Erosion, Himalayan geodynamics, and the geology of metamorphism. *GSA Today*, 11, 4–8.

 45

Captions

	50 km filter	100 km filter	150 km filter
Gibraltar Arc, Spain	7.2 ± 0.6	17.1 ± 0.3	16.3 ± 0.4
Gibraltar Arc, Morocco	6.9 ± 0.6	10.7 ± 0.4	8.0 ± 0.5
Appalachians	19.3 ± 0.4	40.5 ± 0.2	29.2 ± 0.3

Table 1: Root-mean-squared deviation (RMSD) calculated by Equation 2 for each filter wavelength derived synthetic divide, separating the Gibraltar Arc divides into northern and southern sections.

 46

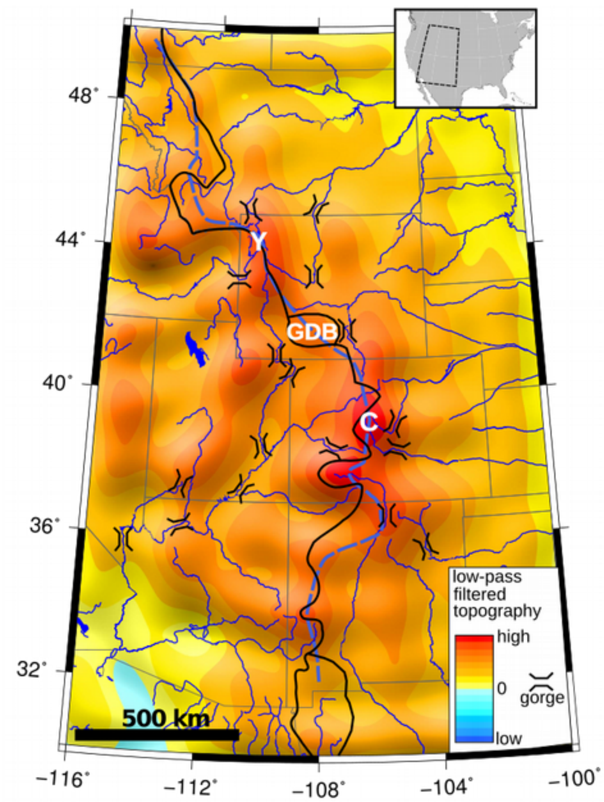

Figure 1: Continental-scale drainage network through the Rocky Mountains of the American west superimposed on low-pass filtered (all wavelengths less than 200 km removed) topography. The actual drainage divide is shown as the black line and the synthetic divide, which is defined by the axis of the long-wavelength topography, is shown by the dashed blue line. Despite the local ruggedness of the topography all major streams begin either in the Yellowstone region (Y) or central Colorado (C) and flow radially away from these topographic highs, locally cutting deep gorges through topography barriers with wavelengths < 200 km, shown with the black symbols. Both of these regions are known to be dynamically-supported by buoyant sub-lithospheric mantle from the Yellowstone hotspot (Pierce & Morgan, 1992) and Rio Grande Rift (Karlstrom *et al.*, 2012), respectively. Note the good general correspondence of the synthetic and actual divide. Note also the Great Divide Basin (GDB) in southwest Wyoming, a region of internal drainage perched atop the long-wavelength topography.

47

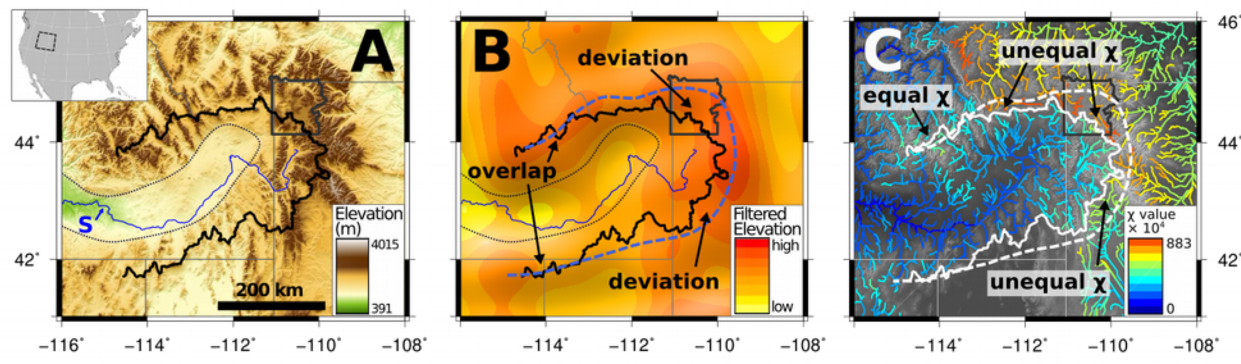

Figure 2: A) Topography, B) low-pass filtered (λ = 150 km) topography, and C) χ value map of the greater Yellowstone region and the Snake River (blue S) plain (after Wegmann *et al.*, 2007). In all figures, the extent of Yellowstone National Park, USA is indicated by the dark gray solid line, and in figures A and B the actual drainage divide of the region is shown by the solid black line and the dotted black line represents the approximate extent of the Snake River Plain. The synthetic divide is shown as the blue dashed line in B, and both the actual and synthetic divides are white in C. Note, the overlap between the actual divide and the synthetic divide through the Snake River Plain where the dynamic topography of Yellowstone decays, and the contrasting poor alignment in the east across the bow-wave of Yellowstone where dynamic topography is growing. The χ map shows disparity (labeled unequal) in channel networks across the divide, with the east-flowing drainages consistently having higher χ values. χ values across the divide in the northwest of the Snake River Plain are approximately equal. Across the divide to the south is an internally drained basin that precludes χ calculations there. The pattern of divide separation and χ values in the Yellowstone region are evidence of the temporal lag in geomorphic processes responding to exogenic forcing.

48

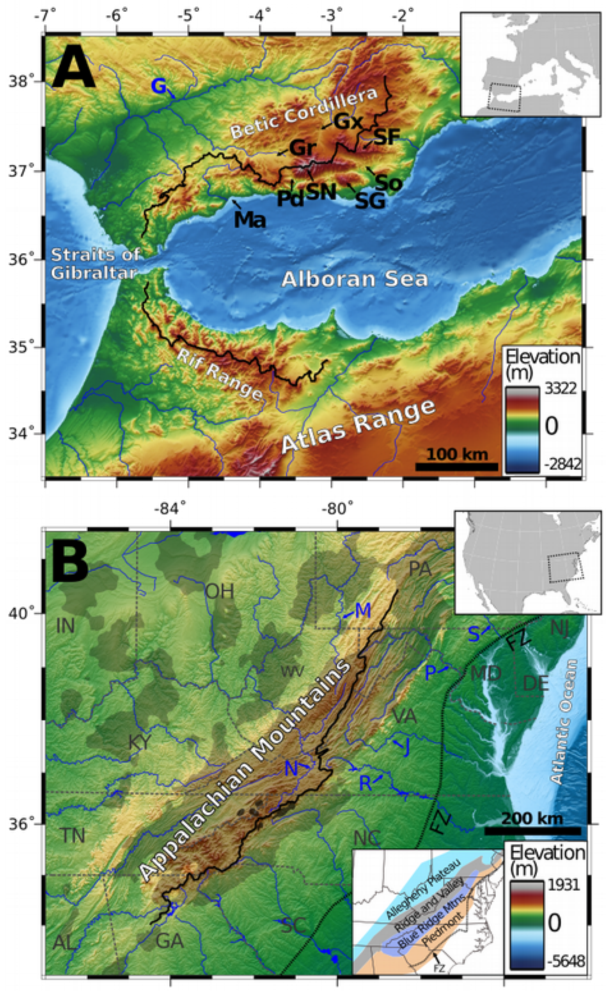

Figure 3: Topographic and drainage maps for A) the Gibraltar Arc and B) Appalachian (Eastern North America) study areas. In both figures the thick black line represents the continental divides. For the Gibraltar Arc, the drainage divide traverses compressional and extensional parts of this actively deforming plate boundary. In the Appalachians, the divide steps westward from the Blue Ridge and Piedmont crystalline rocks in the south into the sedimentary rocks of the Appalachian foreland north of the North Carolina (NC) – Virginia (VA) state line, and then west again into the relatively undeformed foreland sedimentary rocks of the Allegheny Plateau in Pennsylvania (PA). In B, the lightly shaded gray and darkly shaded gray areas represent area contained within the -50 and -100 mGal Bouguer anomaly contours, respectively. Labeled rivers in blue: G – Guadalquivir River, R – Roanoke River, J – James River, P – Potomac River, S –

49

Susquehanna River, D – Delaware River, M – Monongahela River, N – New River. Labeled basins in black: Gr – Granada Basin, Gx – Guadix Basin, So – Sorbas Basin, Pd – Padul Basin. Other features: Ma – Málaga, SN – Sierra Nevada, SG – Sierra de Gador, SF – Sierra de los Filabres. FZ = Fall Zone, thick dotted black line in (B).

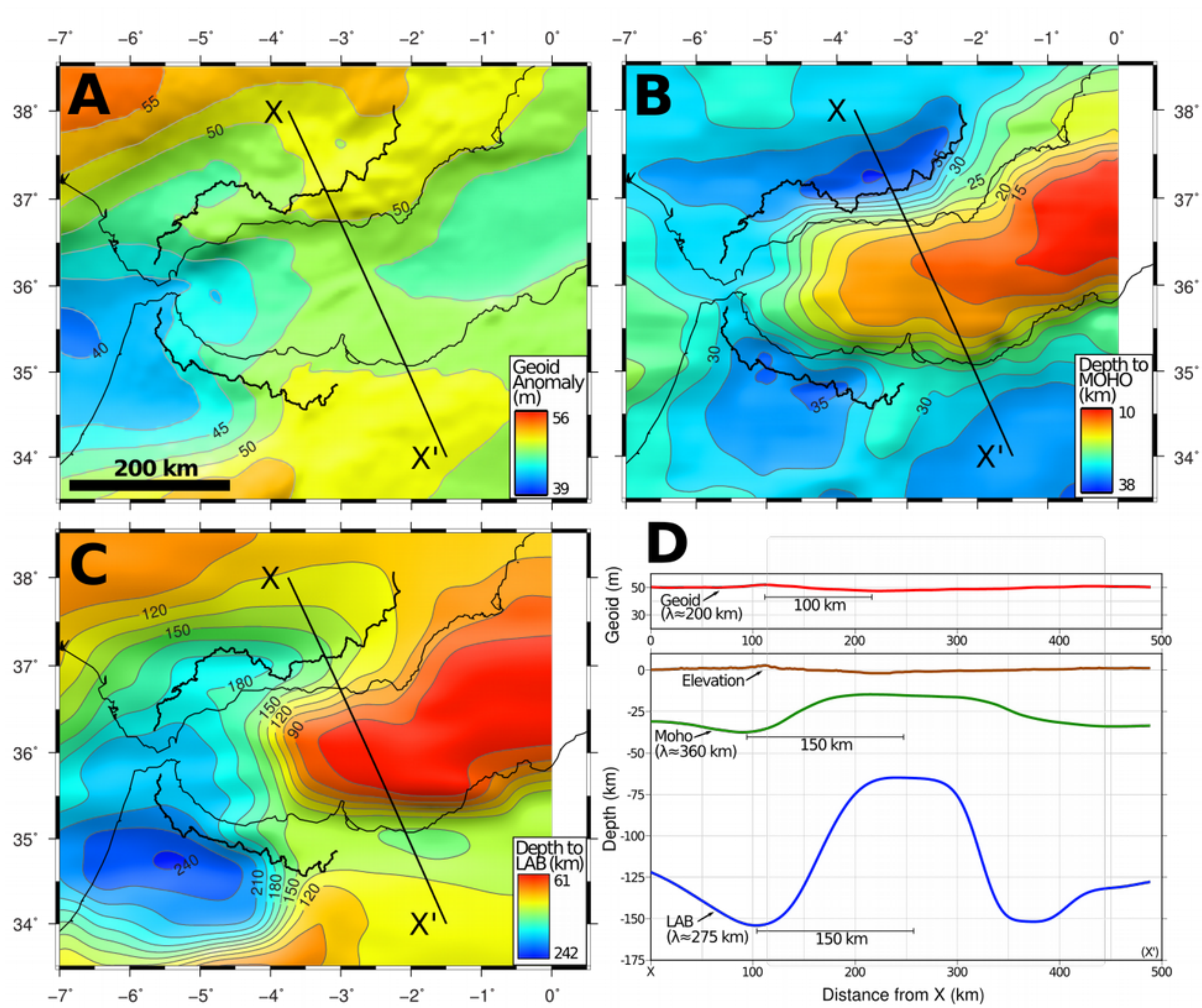

Figure 4: Subsurface characteristics in Gibraltar Arc study setting used to determine threshold wavelength to use in low-pass filtering. A) the geoid anomaly and B) depth to Mohorovičić discontinuity (Moho), from Fullea *et al.* (2010) are interpreted to mostly reflect crustal thickness variations whereas C) depth to lithosphere-asthenosphere boundary (LAB), from Fullea *et al.* (2010) is used to determine changes in the thickness of the lithosphere. D) cross section of

50

datasets along line X to X'. Dataset wavelengths and interpreted half-wavelengths are labeled.

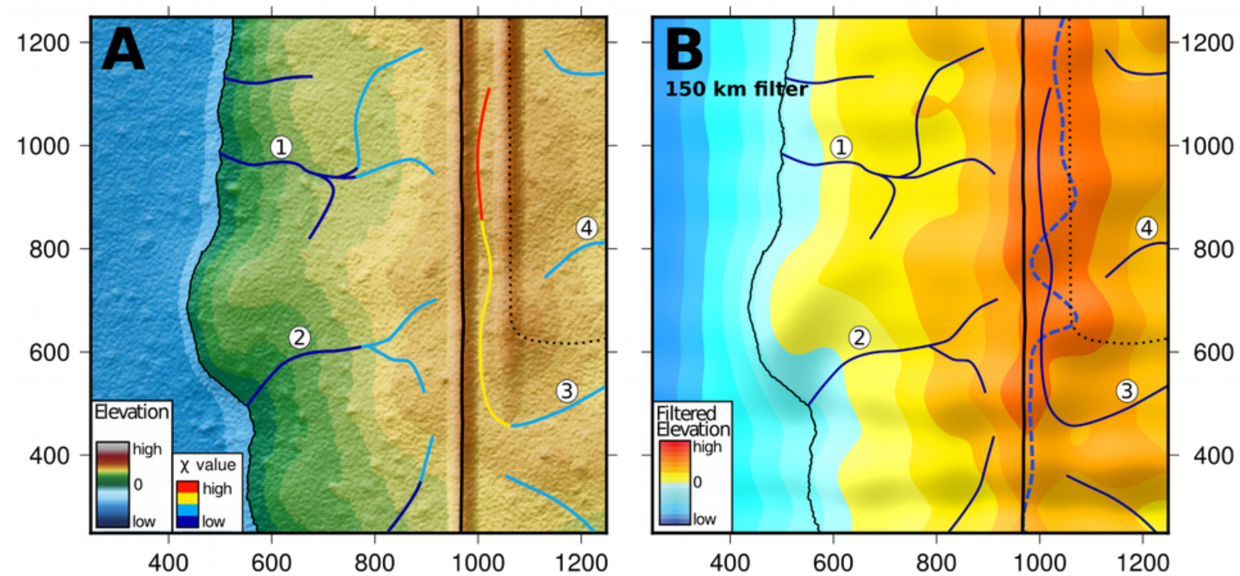

Figure 5: Numerically generated topography used for methodological demonstration of the utility and application of the synthetic drainage divide. A) landscape is produced with a long-wavelength regional gradient, two high parallel ridges, pseudo-random intermediate-wavelength corrugations, and short-wavelength roughness. The shoreline (thin black line), the continental drainage divide (thick black line), and one minor drainage divide (black dotted line) are drawn on the landscape. A hypothetical stream network is drawn to the topography; numbered channel networks are referred to in the text, and stream segments are colored by expected χ values. This reveals relatively high χ values for the headwaters of channel 3, as compared to channel networks 1, 2, and 4. B) the landscape is subject to low-pass filtering at 150 km wavelength, and the parallel ridges are reduced to one broader long-wavelength high. This example demonstrates the emergence of long-wavelength topography from the intermediate and short-wavelength components and the ability to identify the synthetic divide shown as the thick blue dashed line on the crest of the regional topography. This simulation predicts that channel network 3 is likely to be subject to drainage piracy by channel network 1 and/or 2, as the continental divide migrates off the western ridge and nucleates on the crest of the regional high-standing topography.

51

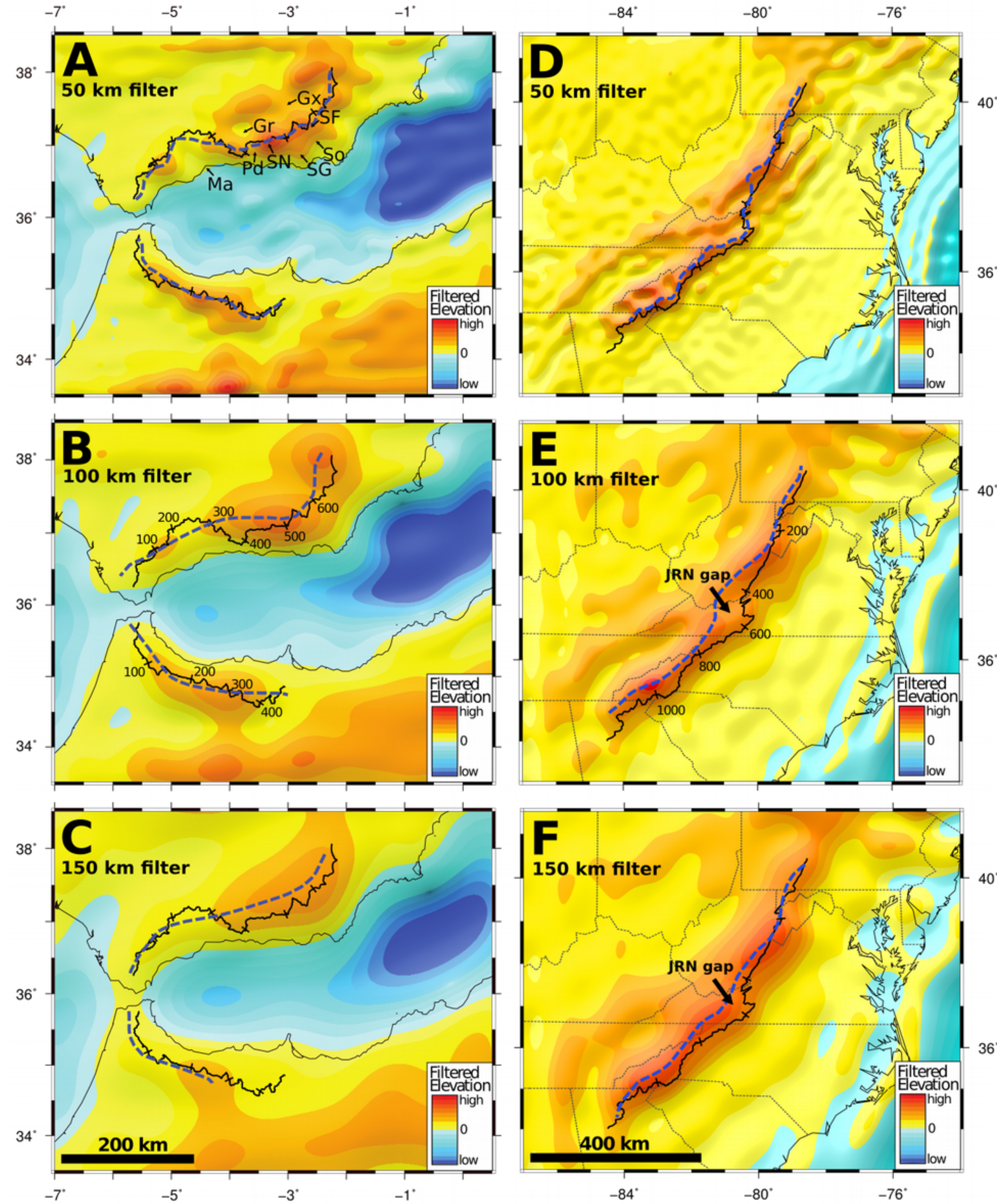

A
50 km filter
Gx
SF
Gr
So
Pd
SN
SG
Ma
B
100 km filter
100
200
300
400
500
600
C
150 km filter
200 km
D
50 km filter
E
100 km filter
JRN gap
1000
F
150 km filter
400 km
Filtered Elevation
high
0
low

52

Figure 6: Low-pass filter results for the Gibraltar Arc (left) and Appalachian study settings (right). In all figures, the thick black lines are the actual continental divides and the blue dashed lines are the synthetic divides derived from the filtered topography. A) Gibraltar 50 km filter, note overall good alignment of the divides. B) Gibraltar 100 km filter, note undulating separation in Spain. C) Gibraltar 150 km filter, note significant separation in SE Spain, but good alignment elsewhere. D) Appalachian 50 km filter, note overall good alignment between divides. E) Appalachian 100 km filter, note the significant separation of the divides in the central Appalachians, labeled as the James-Roanoke-New (JRN) rivers gap. F) Appalachian 150 km filter, note significant and complete separation of the synthetic divide to the west of the actual divide, for the entirety of the central and southern Appalachians. Tick marks along actual divides (labeled in B and E) correspond to the cumulative along-divide distances (km) plotted in Figs. 7 and 8.

 53

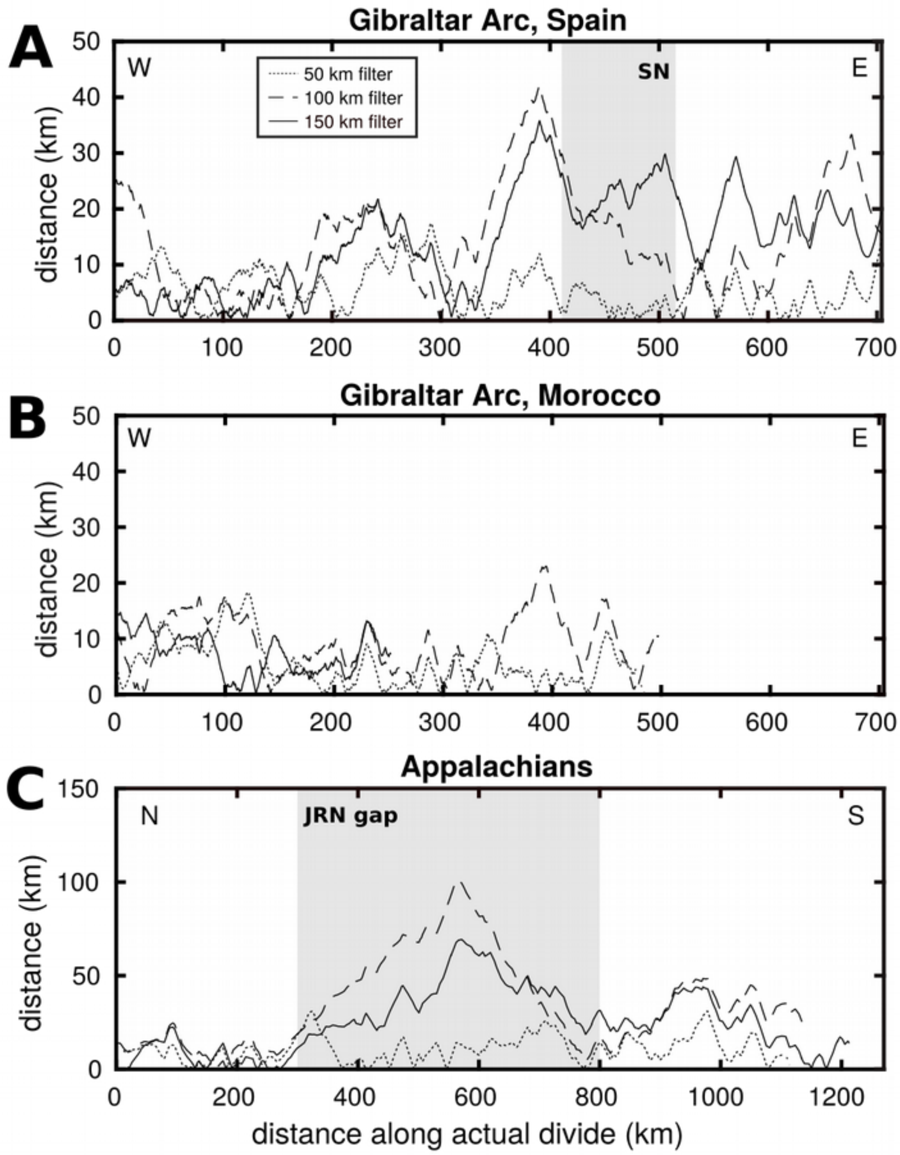

Figure 7: Deviation between synthetic and actual divide calculations plotted along the divide. A) Gibraltar Arc, Spain section of the divide. Divide separation is maximized along the eastern end of the divide, beginning near the Sierra Nevada range (shaded region labeled SN). B) Gibraltar Arc, Morocco section of the divide. Divide deviation is small along the entire length of the divide, and varies without an apparent trend. C) Appalachian divide deviation showing maximum area of separation in the central (north to south) section, herein named the James-Roanoke-New (JRN) gap (shaded region).

 54

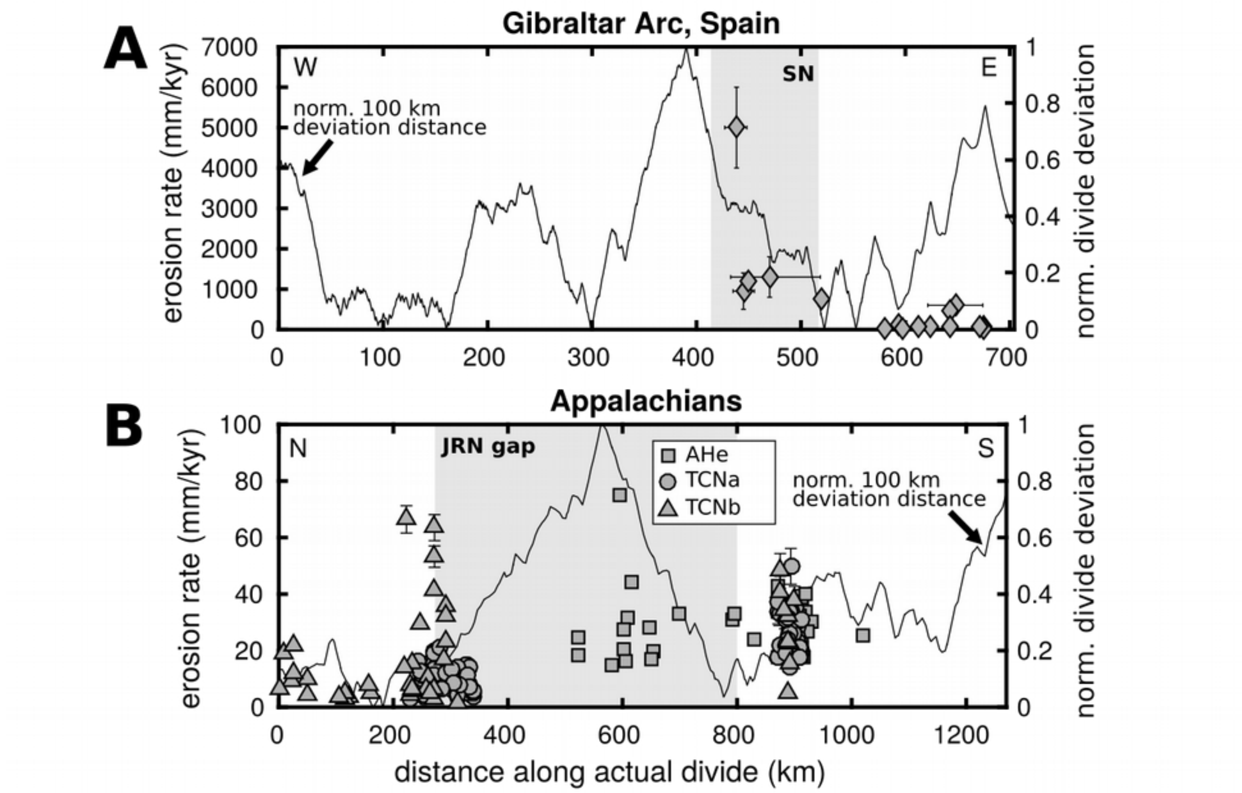

Figure 8: Denudation rate data (see text and Supplementary Tables S1 and S2) compiled from previous research and projected to the divide by interpolation of longitude or latitude for W-E trending or N-S trending divides, respectively. A) erosion rates for Gibraltar Arc, Spain section, and B) erosion rates for Appalachian study area, where data type is denoted by the various symbols. For both figures, vertical error bars indicate uncertainty following the publishing authors notation (error bars are not shown where not reported or smaller than symbol). Horizontal error bars represent a spatial aggregation of measurements that make up a single data point. Solid black line is the synthetic divide deviation of the 100 km filter from each study setting (Fig. 7) normalized to the minimum and maximum deviations as 0 and 1, respectively. This line is to meant to aid in guiding the eye to the areas of higher and lower divide separation when interpreting spatial variability in erosion rate data.

55

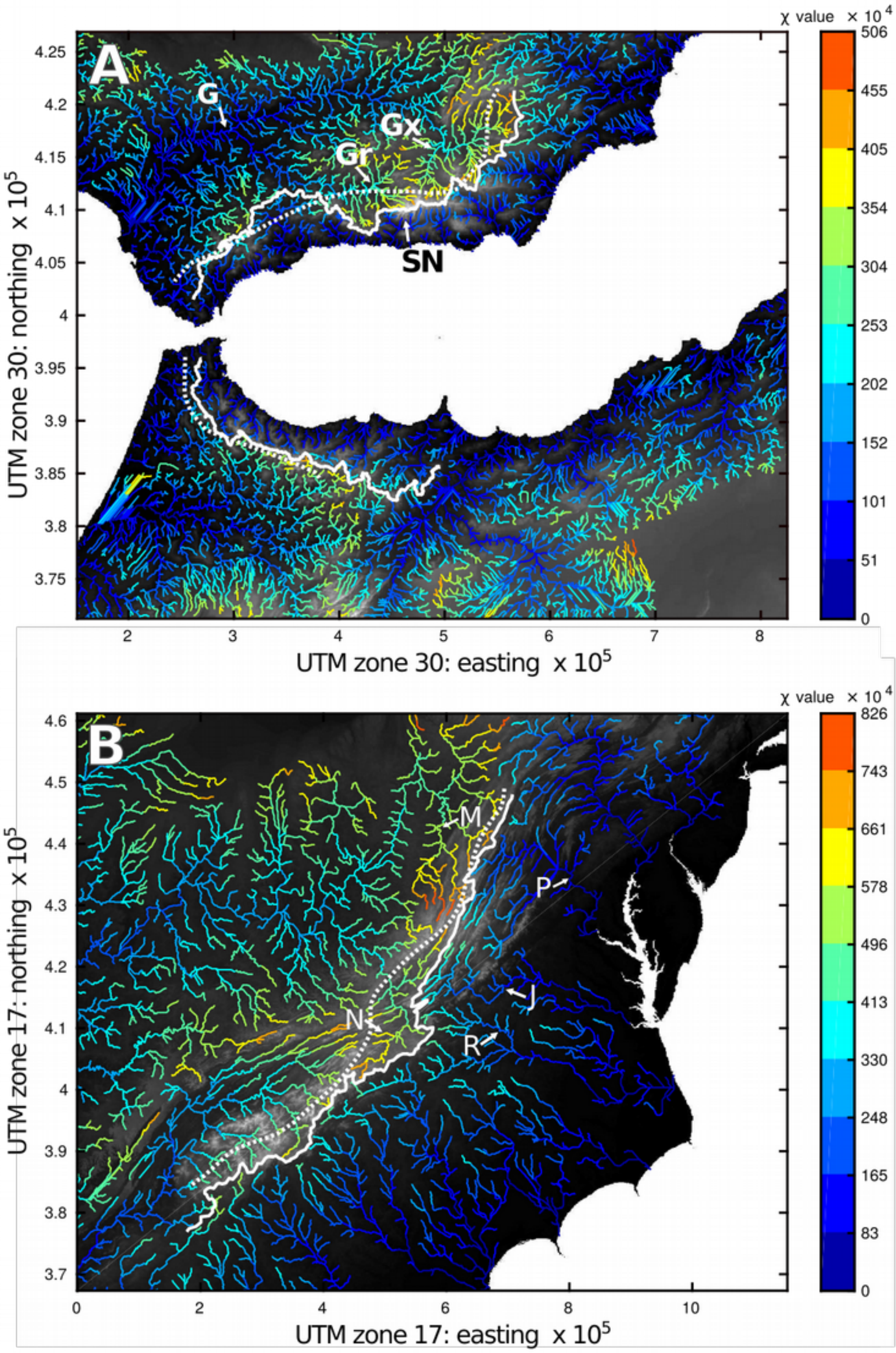

Figure 9: χ transformation of channel networks for study areas; A) Gibraltar Arc study area, and B) Appalachian study area. In both figures, the solid white line is the mapped actual divide, and

56

the white dotted line is the synthetic divide derived from the 100 km filter threshold. The figures are projected in the Universal Transverse Mercator projection, but have approximately the same extent as the other figures in this study. Background is GEBCO digital elevation model with a color gradient going from black to white for low to high topography respectively. Labels are the same as in Fig. 3. Note disparity in χ values calculated across the east end of the Gibraltar Arc, Spain section of the divide that is generally co-located with the length of the divide with the highest calculated deviations. In the Appalachians, the χ values calculated are consistently higher to the west of the continental divide. High χ values can be interpreted as areas poised to be captured by pirating drainage basins.

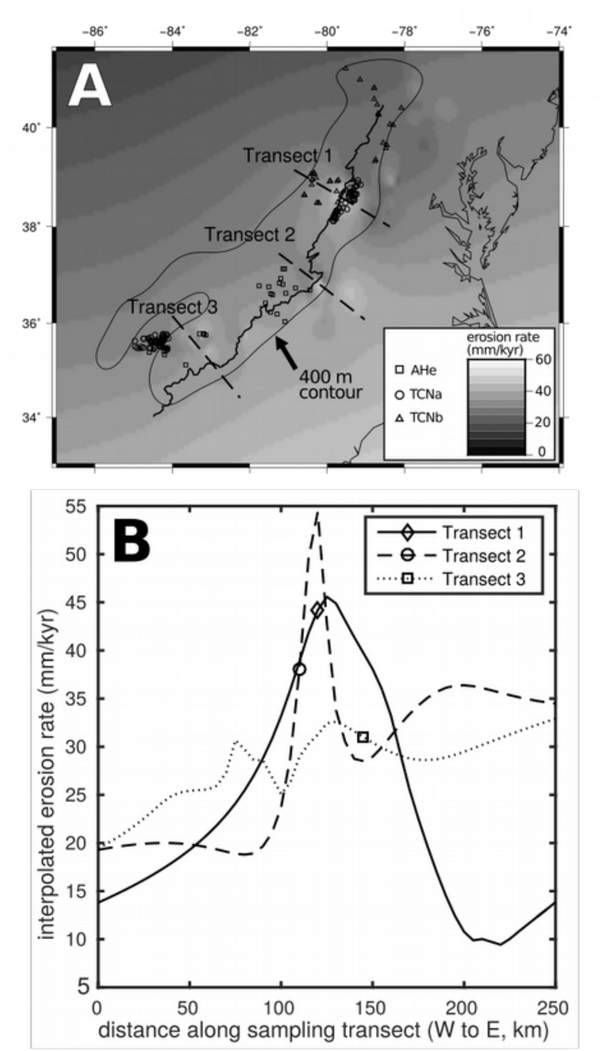

 57

Figure 10: A) interpolated surface of Appalachian erosion data compiled in Supplementary Table S2 and shown in Fig. 8C. See supplementary material for description of spline surface fitting. Black symbols denote locations and type of erosion data, the thick black line is the actual Appalachian continental divide, and the thin black line is the 400 m contour of the 150 km filtered DEM (Fig. 6F) included to guide the eye to the approximate extent of the Appalachians. The surface is sampled along three 250 km transects (dashed lines) positioned orthogonal to the divide in the locations with the most constraining data. B) sampled data from the three transects. Symbol on each line represents the location of transect-and-divide intersection.

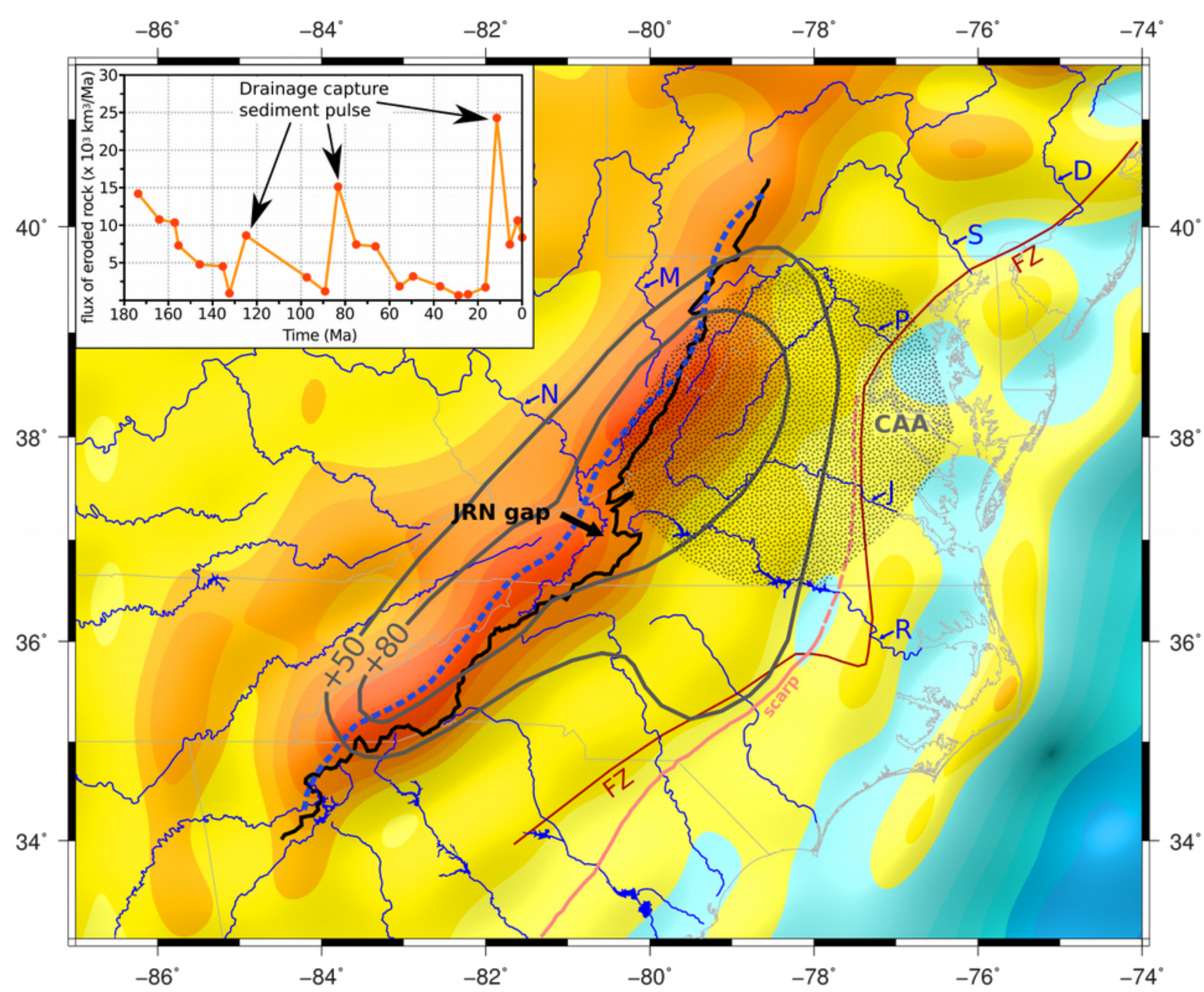

Figure 11: Appalachian 150 km filter overlain with contours of calculated total rock deformation

58

(thick gray lines) since 3.5 Ma, resulting from the combined effects of mantle induced dynamic topography and the flexural response of the lithosphere to unloading and loading of sediments across the surface (Moucha & Ruetenik, 2017). Prince *et al.* (2011) suggest that the Roanoke River (R) will eventually capture the headwaters of the New River (N), causing the actual divide to jump farther west, ultimately approaching or reaching the synthetic divide. This prediction is consistent with patterns of rock deformation (Moucha & Ruetenik, 2017) and calculated χ values (Fig. 9), and crudely co-located with the Central Appalachian Anomaly (CAA) tomographically imaged by Schmandt & Lin (2014). Inset shows the record of sediment flux off the Appalachians into the Atlantic passive margin Baltimore Canyon Trough basin (Pazzaglia & Brandon, 1996). The unsteady flux is characterized by pulses in increased sediment deposition that are interpreted to result from large-scale drainage captures that rapidly incise an enlarged Atlantic slope drainage area. FZ – Fall Zone, scarp – Orangeburg, Chippenham, and Thornburg scarps from Rowley *et al.* (2013).

59